

ABSTRACT

Title of Thesis: **LARGE EDDY SIMULATION
OF A NONREACTING JET**

Christopher M. Briggs Jr., Masters of Science, 2015

Thesis directed by: Professor Arnaud Trouvé
Department of Fire Protection Engineering

Simulations of a turbulent momentum driven jet are carried out by Fire Dynamics Simulator (FDS). These simulations challenge the capabilities of FDS and identify strengths and weaknesses within its code; three bugs were discovered and new user controls were developed. Simulations show that mean and fluctuation vertical velocities and mean mixture fraction radial profiles at locations $z/D=4, 15,$ and 30 are well-captured; however, mixture fraction fluctuations are over predicted at these elevations. Additionally mean vertical velocity predictions are artificially lower above the jet nozzle. These simulations are incorporated into the FDS validation suite.

LARGE EDDY SIMULATION OF A
NONREACTING JET

by

Christopher M. Briggs Jr.

Thesis submitted to the Faculty of the Graduate School of the
University of Maryland, College Park in partial fulfillment
of the requirements for the degree of
Master of Science
2015

Advisory Committee:

Professor Arnaud Trouvé, Chair/Advisor

Dr. Randall J. McDermott, Co-Advisor

Professor Andre W. Marshall

© Copyright by
Christopher M. Briggs Jr.
2015

Acknowledgments

I would first like to thank my wife and family for being supportive and understanding during the past two years. Growing our child, during the most intense time of this research, was not easy. It is your continued patience, love, and understanding that reaffirms why I want to grow old with you.

I would like to thank my advisor Dr. Arnaud Trouvé for his insight and guidance during my completion of this thesis, and his valuable advice throughout my years at the Department of Fire Protection Engineering. I would also like to thank my co-advisor, Dr. Randall McDermott. Having the opportunity to work with him and the FDS development team at NIST, was an experience that will remain with me and continue to shape me in my career. This thesis would not have had the impact, as minimal as it might be, without his extraordinary guidance, ideas and computational expertise. I would also like to express my gratitude to Dr. Andre Marshall, for agreeing to serve on my thesis committee and for sparing his time and effort in reviewing my work. Lastly, I would like to thank the FDS development team for their administrative, professional, and personal time.

Table of Contents

List of Figures	v
List of Abbreviations	vii
List of Symbols	viii
1 Introduction	1
1.1 Motivation for this study	1
1.2 Fire Dynamics Simulator	5
1.3 The Application of FDS to Jet Fire Simulations	6
1.4 Literature Review	6
2 Experimental and Simulation Setup	10
2.1 Experimental Setup	10
2.2 Experimental Data	11
2.3 Length Scale Considerations	17
2.4 Time Scale Considerations	19
2.5 Simulation Configuration	19
2.6 Boundary Conditions	23
3 Results and Discussion	26
3.1 General Information	26
3.2 Inlet Boundary Conditions	26
3.3 Centerline Profiles	29
3.4 Radial Profiles	31
3.5 Statistical Convergence	37
3.6 Filtered Considerations	37
3.7 Profile Error	39
3.8 Vorticity at the Boundary	40
3.9 Viscosity at Mesh Boundaries	43
4 Conclusion	45

A	Contributions	47
B	Testing Jet Boundary Conditions	48
B.1	Introduction	48
B.2	2-Dimension Test Simulations	48
B.3	Axisymmetric Test Simulations	49
B.4	3-Dimension Test Simulations	56
C	FDS Input Files	65
C.1	Course Resolution FDS Input File	65
C.2	Medium Resolution FDS Input File	71
C.3	Fine Resolution FDS Input File	76
	Bibliography	83

List of Figures

2.1	Experimental setup	11
2.2	Experimental centerline mean vertical velocity vs. theory	12
2.3	Experimental centerline mean mixture fraction vs. theory	13
2.4	Experimental radial profile of mean vertical velocity vs. theory	14
2.5	Experimental radial profile of mean mixture fraction vs. theory	15
2.6	Experimental radial profile of mean radial velocity vs. theory	16
2.7	Various length scales and ranges of eddies	18
2.8	Mesh arrangement for FDS simulations	21
2.9	Mesh arrangement for FDS simulations	22
2.10	Simulated jet nozzle and device configuration	23
2.11	Boundary layer profile	25
3.1	Expected vs. FDS Output velocity profile at the jet exit	27
3.2	Mass fraction of propane being issued into the domain	28
3.3	Centerline profiles of velocity and mixture fraction	30
3.4	Decay of centerline profiles of velocity and mixture fraction	30
3.5	Radial vector and scalar profiles at $z/\text{ID} = 4$ above the jet nozzle	32
3.6	Radial vector and scalar profiles at $z/\text{ID} = 15$ above the jet nozzle	34
3.7	Radial vector and scalar profiles at $z/\text{ID} = 30$ above the jet nozzle	36
3.8	Vertical velocity signals at elevations of $z/\text{ID} = 4, 15$ and 30	38
3.9	Corrected centerline profile of velocity	39
3.10	Parabolic velocity profile error	40
3.11	Open boundary vorticity error	41
3.12	Simple graphic of ‘Open’ boundary conditions calculation	42
3.13	Mesh boundary viscosity error	44
3.14	Ghost cells at mesh boundary	44
B.1	2D jet boundary condition test using a parabolic profile where $w_0 = 69$ m/s	49
B.2	Multimesh axisymmetric bug	50
B.3	Axisymmetric jet boundary condition test using the experimental profile at $z/\text{ID} = 4$ where $w_0 = 69$ m/s	52

B.4	Axisymmetric jet boundary condition test using a parabolic profile where $w_0 = 69$ m/s	53
B.5	Axisymmetric jet boundary condition test using a parabolic profile at two different resolutions	54
B.6	Axisymmetric jet boundary condition test using a parabolic profile where the maximum velocity is specified as $2u_{bulk}$ and transport coefficients were specified.	55
B.7	Jet boundary condition test using the experimental mass flux at the boundaries	56
B.8	Jet boundary condition test using a flat profile with a specified velocity of 53 m/s.	57
B.9	Jet boundary condition test using a flat profile with a specified velocity of 69 m/s.	57
B.10	Comparison of mass flux, flat velocity, and parabolic velocity profiles	58
B.11	Jet boundary condition test using the experimental profile with a turbulence forcing of 10 m/s at the boundaries; $w_0 = 69$ m/s	59
B.12	Jet boundary condition test using the experimental profile with a turbulence forcing of 5 m/s at the boundaries; $w_0 = 69$ m/s	60
B.13	Jet boundary condition test using the experimental profile with a turbulence forcing of 3 m/s at the boundaries; $w_0 = 69$ m/s	60
B.14	Comparison of the effects of turbulent forcing on vertical mean and RMS velocities	61
B.15	Jet boundary condition test using the experimental profile with a turbulence forcing of 5 m/s at the boundaries; $w_0 = 85$ m/s	62
B.16	Jet boundary condition test using the experimental profile with a turbulence forcing of 5 m/s at the boundaries and using the Dynamic Smagorinsky turbulence model	63
B.17	Jet boundary condition test using a flat profile with a specified velocity of 85 m/s.	63
B.18	Jet boundary condition test using a parabolic profile where the centerline velocity is specified as $2u_{bulk}$	64

List of Abbreviations

API	American Petroleum Institute
CFD	Computational Fluid Dynamics
FDS	Fire Dynamics Simulator
FR	Federal Register
IBC	International Building Code
LDV	Laser Doppler Velocimeter
LES	Large Eddy Simulation
MSC	Maritime Safety Committee
NRC	Nuclear Regulator Commission
NFPA	National Fire Protection Association
PBD	Performance Based Design
RANS	Reynolds Averaged Navier Stokes
SFPE	Society of Fire Protection Engineers
SOLAS	Safety of Life at Sea
USCG	United States Coast Guard

List of Symbols

F	mixture fraction
Fr	Froude number
g	acceleration due to gravity
ID	jet nozzle inner diameter
k	kinetic energy
L	half length
l	eddy length
OD	jet nozzle outer diameter
RMS	root mean square value
r	radial position
R	jet nozzle radius
Re_D	Reynolds based on mean velocity and nozzle inner diameter
w	vertical velocity
u	radial velocity
z	vertical coordinate
δ	boundary layer thickness
δ_ν	viscous length scale
η	Kolmogorov length scale
μ	dynamic viscosity
ν	kinematic viscosity
ρ	density
τ	stress
$\langle \Phi \rangle$	mean quantity
Superscript	
$\bar{\Phi}$	filtered quantity
Φ'	fluctuation
Subscript	
$Bulk$	bulk value
rms	root mean square
c	denotes centerline value
e	denotes quantities of the coflow
j	denotes quantities of the jet
0	maximum value
sgs	sub-grid scale
τ	denotes friction value
w	wall value

Chapter 1: Introduction

1.1 Motivation for this study

As industry advancements continue to outpace government regulations, administrative authorities are increasingly adopting performance based design (PBD) criteria when accepting industry's novel developments in the construction of facilities, structures, and vessels. An important tool for determining design performance is the use of various types of modeling techniques to evaluate key parameters outlined by regulator requirements. Examples of regulatory authorities accepting PBD criteria include: the wide acceptance of the International Building Code (IBC) and the various allowances for PBD [1]; the Nuclear Regulatory Commission's (NRC) adoption of the National Fire Protection Association (NFPA) standard 805 regarding Performance-Based Standards for Fire Protection for Light-Water Reactor Electric Generating Plants [2]; and the United States Coast Guard's (USCG) adoption of the SFPE Engineering Guide to Performance-Base Fire Protection Analysis and Design of Buildings which accepts PBD criteria on United States vessels sailing in foreign waters. (MSC Cir/1002 Navigation and Vessel Inspection Circular (NVIC) 6-02) [3].

The USCG has continued to publish and accept PBD criteria when granting

regulatory approval to new ship constructions. In response to the explosion, fire and sinking of the mobile offshore drilling unit DEEPWATER HORIZON, the USCG recently provided industry with recommended interim voluntary guidelines for the fire and explosion analysis onboard manned fixed and floating offshore facilities and mobile offshore drilling units. These interim guidelines were provided to industry in expectation of future proposed rule making, which would make such recommendations mandatory. As these are interim guidelines, the USCG has urged owners and operators on the outer continental shelf to voluntarily comply with the published recommendations to adequately protect personnel and safety-critical spaces and elements located onboard assets. The USCG has emphasized that compliance with the recommended measures will ensure increased protection against potential fire and explosion scenarios following a serious casualty event, such as the loss of well control [4].

The interim measures recommended by the USCG include an engineering evaluation of fire and blast loads in the design of offshore facilities based on the fire and explosion risk of hydrocarbon fuel sources. These evaluations should identify hazards and potential damage of major casualties. To optimize their effectiveness and utility, evaluations should consist of hazard identification, consequence evaluation, adequacy of control and mitigation measures, and final risk assessment. A thorough evaluation should also include an establishment of accepted performance criteria to demonstrate that appropriate mitigating measures have been implemented for the protection of the facility and personnel. When conducting these engineering evaluations, the USCG has adopted the American Petroleum Institute's (API) Rec-

ommended Practice 2FB [4].

API's Recommended Practice 2FB standard notes that the radiant heat flux produced from jet fires may be on the order of 300 KW/m² in open conditions and up to 400 KW/m² confined areas. The standard provides engineering correlation for the prediction of jet geometry and radiative energy release rates. In response to these engineering correlations, owners and operators employ various tools and models to predict flame geometries and heat release rates from jet fires and use those results to persuade stakeholders in the approval of a design, arrangement, or operational stipulation [4].

Two main types modeling techniques have been implemented by fire protection engineers: zone models and computational fluid dynamics (CFD) models. Zone models, for fire protection applications, divide the model space into different control volumes, or 'zones'. When used by fire protection engineers, zone models are commonly divided into two spaces: 1) a hot upper gas layer and 2) a cooler lower layer [5]. Zone models are not the preferred method for attempting to characterize a hazardous scenario due to a jet fire because these models are ineffective for detailing essential elements critical to the assessment of jet fires. Because these essential elements are lacking in zone models, CFD models are more adept at simulating and predicting jet fires.

CFD models solve systems of equations, often using Navier Stokes equations to obtain increased average quantities. Two types of CFD models are predominately used by fire protection engineers: Reynolds Average Navier Stokes (RANS) and Large Eddy Simulation (LES). RANS simulations are a practical alternative to sim-

ulate high speed flows in engineering applications to zone models as they are more detailed than zone models and a cheaper alternative to LES. RANS simulations resolve the mean flow and use a turbulence model to present system turbulence. RANS methods are computationally cheap, making it an appealing mode to industry for all kinds of engineering problems. Despite the appeal of RANS to industry, LES is a more complex modeling technique that better describes the turbulent nature of various profiles. LES spatially filters the equations of motion and resolves eddies larger than the filter size; eddies that are smaller than the filter size are described using subgrid models. An advantage of LES models is their ability to describe turbulence that are of the similar scale as the grid size. Although the cost of a LES far exceeds that of a RANS simulation, and the cost difference increases with increasing Reynolds number, LES is the preferred modeling technique as it provides far greater detail and more effective analysis and prediction of jet fires [6].

Based on the aforementioned benefits, LES models and codes are widely adopted for practical engineering applications as computing power has significantly increased over the past three decades and because LES codes provide more insight in the dynamics of simulated problems. But, not all LES codes are equal. Before an owner, operator, stakeholder, or regulator should consider results from an LES code (or any code), the code must be thoroughly verified and validated. One such validated code is the Fire Dynamics Simulator (FDS), which is an open source, widely used, LES code created for fire applications and is discussed in greater detail below.

1.2 Fire Dynamics Simulator

FDS is a CFD model designed to model combustion and fire driven flows. FDS numerically solves the low Mach formulation ($Ma < 0.3$) of the Navier-Stokes equations that most appropriately describe the flow of fire, heat transfer and smoke transport. FDS was created by and is maintained by a deployment team at the National Institute for Standards and Technology (NIST), a U.S. government organization with other private and public contributors to the code. The code is open source and, as of the date on this document, can be obtained at <https://code.google.com/p/fds-smv/> [7].

FDS's default code is a low Mach LES with explicit, second-order numerics to conserve kinetic energy. It has a structured, uniform, staggered grid, and utilizes a lumped species method to simplify chemistry and scalar (species) transport. By default, FDS uses the eddy dissipation model, which treats all reactions (unless specified) as a single step reaction between fuel and oxidizer (mixed is burned). The radiation model implements a grey gas assumption with a finite volume solution to radiation transport. The default turbulence model is the Deardorff eddy viscosity for subgrid scales with constant turbulent Schmidt and Prandtl numbers [7].

The code is not limited to the above description of mathematical models and numerical schemes. The hydrodynamic model, combustion model, and radiative transport can be varied. Additionally, boundary conditions can be varied to compute empirical correlations, or heat and mass transfer directly when performing a Direct Numerical Simulation (DNS). The complete formulation of these equations and the

numerical methods used for these equations are described in the FDS Technical Reference Guide. [8].

1.3 The Application of FDS to Jet Fire Simulations

The research presented in this paper creates a validation case to demonstrate FDS's capability to simulate a momentum driven flow. FDS has a suite of over 2000 validation simulations, which are included in multiple cases. In FDS's validation suite, there is a set of test cases dedicated to the purpose of comparing various turbulence models and their predictions on a jet's centerline velocity and decay. These set of cases simulate a jet modeled with $Re=10,000$ [8]. While this jet is turbulent, its velocities are not nearly as high as potential jet fires that could occur on offshore drilling or production assets. Before using FDS and applying it to a potentially more severe, realistic scenario, and before attempting to validate the correlation in API RP 2FB, a validation case needed to be created to verify FDS's ability to model high speed flows (speeds higher than normal pool fire plume velocities and lower than 0.3 Mach). The validation case in this research tested FDS's capability at simulating high speed flows, using a well-characterized, nonpremixed, nonreacting, propane jet issued into a coflow airstream.

1.4 Literature Review

Extensive studies have been conducted of jets with constant density, but variable-density jets are less well studied; only a few experimental studies are re-

ported for such cases. Sandia Laboratories conducted a study where LDV and Raman scattering was used to interrogate a nonpremixed variable density jet with a propane jet (bulk velocity of 53 m/s) issuing into a coflow of air with a velocity of 9.2 m/s [9]. This study is desired as it is one of the sole jets studies that has higher speed velocities which is still be able to be used when appemiting a simulation using a low Mach code. Gouldin et al. used a second order closure model was used to calculate the mixing of this jet [10]. Little information was given to describe the inlet boundary conditions used while performing this calculation. No other literature could be found for the simulation of this experiment.

Djeridane et al. performed studies of variable density jets, to include helium, air and CO2 jets issuing into a low speed coflow of air [11]. Numerical simulations of these types of flows are also relatively sparse. Gharbi et al. conducted a numerical study of these helium, air, and carbon dioxide in air [12]. They note that they found issues with the area with higher density gradients.

Chen and Rodi propose that a vertical buoyant round jet behaves like a non-buoyant pure jet in the region close to the jet exit where the internal forces are dominate and starts to behave like a pure plume in the far field where the inertial forces of the jet are less a dominate factor [13]. These distances can be assessed by the Froude number at the jet exit

$$Fr = \frac{\rho_e w_j^2}{g|\rho_j - \rho_e|ID} \quad (1.1)$$

where the inertial range extends to

$$X_1 = 0.5IDFr^{.5}(\rho_j/\rho_e)^{.25} \quad (1.2)$$

and the plume range begins

$$X_2 = 10X_1 \quad (1.3)$$

Using the above, the jet exit Froude number for the Sandia nonreacting propane jet is 2.76×10^5 , the inertial region extends to an axial location of $z/D = 1.5$ and the plume region begins at an axial location of $z/D = 15.2$. Chen and Rodi also proposed similarity laws for variable density jets [13]. The proposed solution for mean centerline vertical velocity and mean centerline mixture fraction are

$$w_c/w_j = 6.3(\rho_j/\rho_e)^{.25}(ID/z) \quad (1.4)$$

and

$$F_c/F_j = 5.4(\rho_j/\rho_e)^{.25}(ID/z) \quad (1.5)$$

They also propose an approximate similarity solution which Wang describes as pseudo-similarity solution for radial profiles of mean vertical velocity and mean mixture fraction [14]. This is found to be

$$u(x) = \exp[-x/L]^2 \ln 2 \quad (1.6)$$

Similarity solutions for variable density jet radial velocities was not found.

Pope proposes a radial velocity profile solution for a uniform density jet

$$u(\eta) = \frac{1}{2}(\eta - a\eta^3)/(1 + a\eta^2)^2 \quad (1.7)$$

where

$$\eta = r/(z - z_{or}) \quad (1.8)$$

where z_{or} is the virtual origin (which is $z/ID = 3.0$) [10] and

$$a = (\sqrt{2} - 1)/S^2 \quad (1.9)$$

where

$$S = \frac{dL(z)}{dz} \quad (1.10)$$

This similarity solution is only proposed for regions of $z/ID > 30$. A review of List's Turbulent Jets and Plumes gives a similar solution [15] but no solution is provided for radial velocities in the near field region. Comparisons of centerline vertical velocity and mixture fraction experimental and theoretical decay are shown in Chapter 2. Radial profiles of experimental versus theoretical prediction of mean vertical and radial velocities and mixture fraction are also shown in Chapter 2.

Chapter 2: Experimental and Simulation Setup

2.1 Experimental Setup

All measurements were performed in the Sandia Turbulent Diffusion Flame Facility. A simple schematic of the test section is shown in Fig. 2.1. For a complete description of the test facility, see Dibble *et al* [16]. The test configuration was orientated vertically to minimize asymmetrical effects due to buoyancy. The experimental test section was 30 cm x 30 cm and 200 cm tall. CE Rayleigh scattering was used for single-point density and mixture fraction measurement. Laser doppler velocimetry (LDV) was used to measure simultaneous single point axial and radial velocities. Raman scattering was used for single point species concentrations for propane, combined LDV-Raman for single-point species concentrations and two velocity components and one dimensional Rayleigh imaging for instantaneous radial profiles of density and mixture fraction [16].

The flow configuration consisted of a high velocity round central jet of non-premixed propane surrounded by a coflowing air stream. The fuel nozzle inside diameter (ID) was 5.2 mm with an outer diameter (OD) of 9.0 mm. The jet bulk velocity was 53 m/s with a mass flow rate of 2.3 gm/sec [9]. Bulk velocities of the fuel jet were determined from the measured volumetric flow rates and the inter-

nal area of the jet nozzle. The mass flow rates exiting from the tube was known to 2% [10]. The Reynolds number, based the the nozzle's ID and bulk velocity is 68,000. Ratios of the jet to coflow air velocity (based on the bulk velocity of the fuel jet) was 5.8.

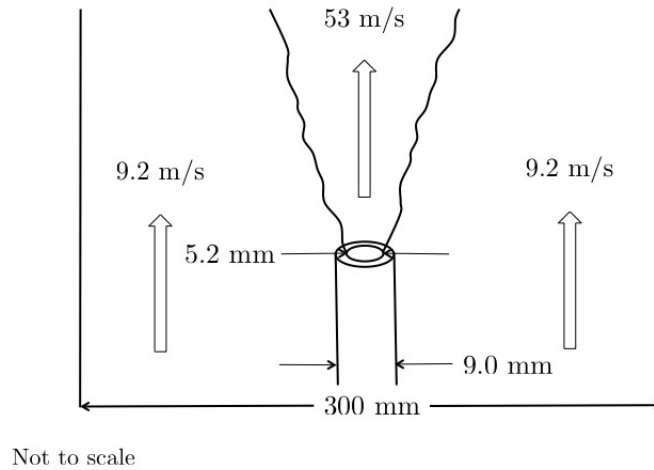


Figure 2.1: Experimental Setup.

2.2 Experimental Data

Mean centerline quantities of vertical velocity and mixture fraction were measured up to 80 diameters for the propane nonpremixed, nonreacting case. Radial profile measurements of the propane jet of vertical mean velocity and fluctuation values, radial mean velocity and fluctuation values at location 4, 15, 30 and 50 diameters downstream [16]. Fig. 2.2 and 2.3 present the experimental centerline mean vertical velocity and mean mixture fraction experimental data compared to

the theory presented in Section 1.4. Fig. 2.4 and 2.5 present the experimental radial mean vertical velocity and mean mixture fraction experimental data compared to the theory presented in Section 1.4. These data are presented in a non dimensional form to show all the profiles at the axial locations of interest ($z/ID = 4, 15,$ and 30). Fig. 2.6 presents the experimental radial profile of radial velocity at an axial location of $z/ID = 30$. This axial location is the sole location the this study’s computational domain where the jet theory can be applied. It should also be noted that this is a comparison of the experimental data to the theory of a uniform density jet; Section 1.4 discusses this further. Experimental data for the nonreacting, non-premixed propane jet can be found on the International Workshop on Measurement and Computation of Turbulent Nonpremixed Flames workshop website. [9].

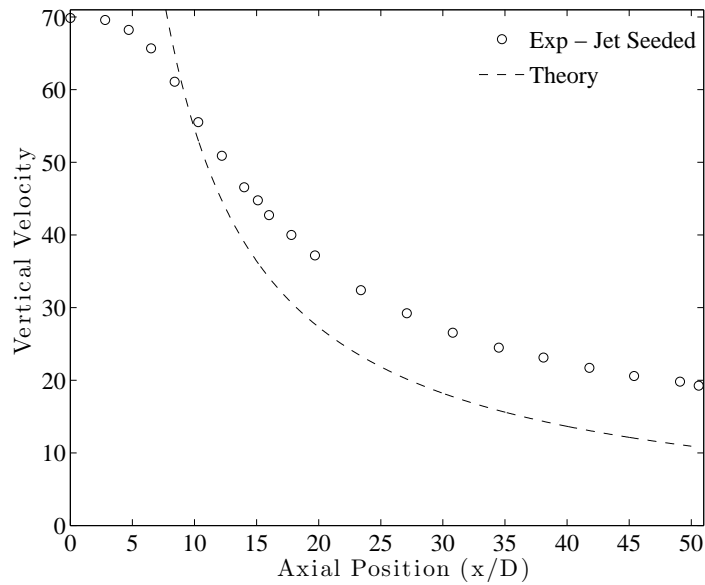


Figure 2.2: Experimental centerline mean vertical velocity data compared to the theoretical solution of a variable density jet.

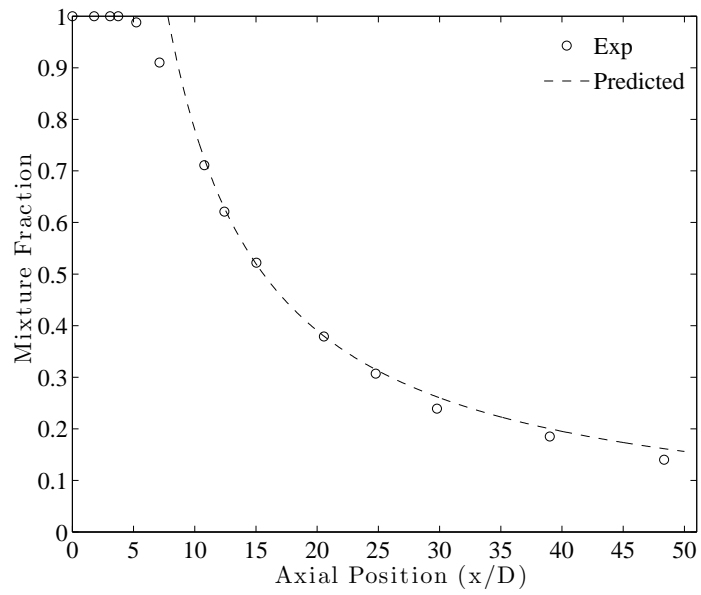


Figure 2.3: Experimental centerline mean mixture fraction data compared to the theoretical solution of a variable density jet.

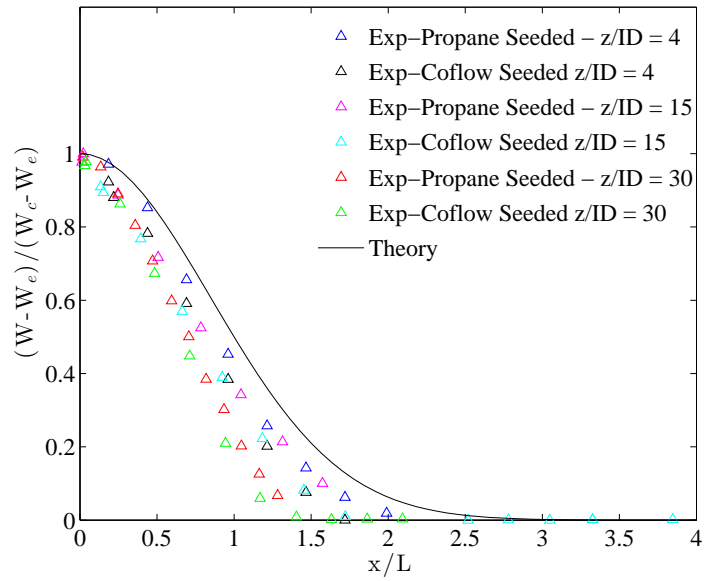


Figure 2.4: Experimental radial profiles of mean vertical velocity data compared to the theoretical solution of a variable density jet. Data includes profiles from axial location of $z/ID = 4, 15,$ and 30 .

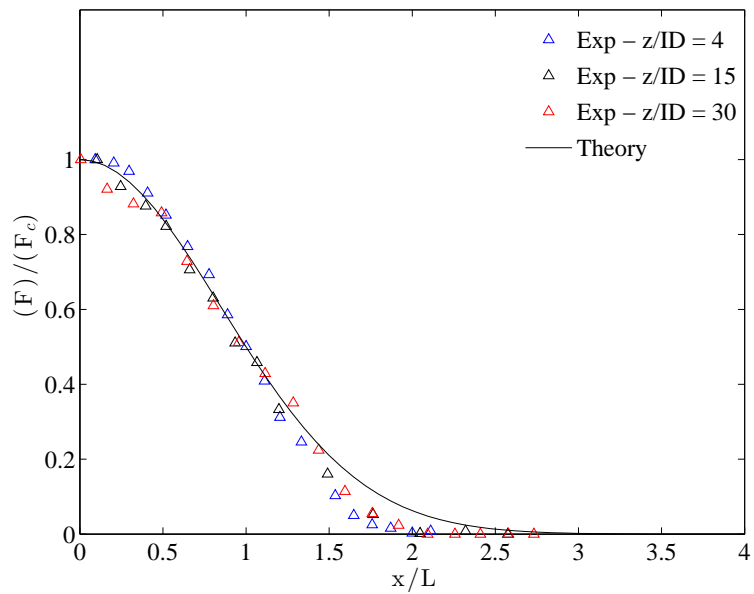


Figure 2.5: Experimental radial profiles of mean mixture fraction data compared to the theoretical solution of a variable density jet. Data includes profiles from axial location of $z/ID = 4, 15,$ and 30 .

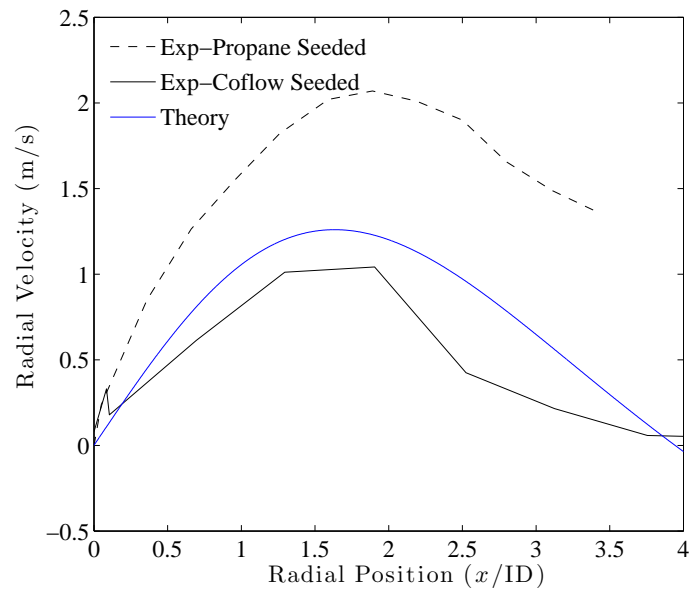


Figure 2.6: Experimental radial profiles of mean radial velocity data compared to the theoretical solution of a jet.

2.3 Length Scale Considerations

In LES, all length scales should be considered before establishing the grid and filter spacing. Kolmogorov hypothesized that at sufficiently high Reynolds number, the small scale turbulent motions are statically isotropic. He goes on to hypothesize that the statistics of the motions of the lengths above the inertial subrange are uniquely characterized by the kinetic energy dissipation rate (ε) and the viscosity (ν) and that at lengths below the inertial subrange, but above the Kolmogorov length (η), the characterization of the turbulent flow is determined by the dissipation energy (ε) and independent of viscosity (ν). Fig. 2.7 shows the various length scales and ranges of eddy sizes (on a logarithmic scale) where l_E is the length where eddy sizes shift from the energy contain range to the inertial range and l_D is the length where eddies transition from the internal range to the dissipative range [17].

Eddies of length η can be estimated by

$$\frac{\eta}{l_0} \approx \text{Re}^{-3/4} \quad (2.1)$$

as provided by Pope [17]. Assuming that l_0 can be approximated by the ID of the jet, then the smallest scale to resolve in this configuration would be on the order of 1×10^{-6} .

In the case of the nonpremixed, nonreacting, propane jet, three characteristic length scales are considered; geometry of the bulk flow, boundary layer (δ), and viscous length scale (δ_ν). The bulk flow length is set by the physical arrangement of the experiment, the ID of the tube (see Fig. 2.1). The boundary layer of the

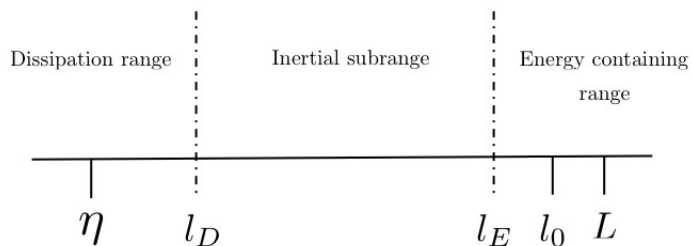


Figure 2.7: Various length scales and ranges (on a log scale) of eddies sizes (l) at high Re numbers.

flow can be seen in Fig. 2.11 and is described by Eqn 2.4. This boundary layer will be described in more detail in a later sections. In the simulation configuration, the boundary layer thickness is found to be 6.5×10^{-4} m.

The smallest length scale to consider is the viscous length scale

$$\delta_\nu = \frac{\nu}{u_\tau} \quad (2.2)$$

where $u_\tau = \sqrt{\tau_w/\rho}$ and $\tau_w = \mu \partial u / \partial r$ [8]. δ_ν is approximated to be 10^{-6} which is the same order of magnitude as the smallest scales predicted by Kolmogorov. Simulations are run with grid sizes of $ID/\Delta = 8, 16,$ and 32 . These grid resolutions are chosen due to time allowance and computational availability. For a truly well resolved LES simulation, the boundary layer (δ) should be resolved with ten grid points; a resolution of $ID/\Delta = 80$ would be needed to resolve this layer. This is

computationally expensive, and due to resource issues and time constraints, $ID/\Delta = 32$ is the finest resolution that can be achieved at this time.

2.4 Time Scale Considerations

The vector quantities of concern in this simulation are mean and fluctuating vertical and radial velocities. The duration of the simulation is determined by the mixing time of the propane jet in air [17]. Experimental data are used to estimate a mixing time at $z/ID = 30$, the location with the lowest velocity magnitudes and largest plume width; this time is 8×10^{-3} s. The start time for gathering statistics is determined by the flow-through times of the propane using the centerline velocity at $z/ID = 30$; this flow-through time is 6.6×10^{-3} s. Ten cycles were desired to ensure convergence of the mean and fluctuating quantities. A run time of 0.1 s is selected with statistics collection at 0.01 s.

FDS controls the time step for each simulation so that

$$\Delta t = C_{max} \frac{\Delta x}{u} \quad (2.3)$$

where C_{max} is increased or decreased to remain between 0.8 and 1.0. The time step can be controlled, but was left to the default for this simulation [8]. The time step in the simulations are on the order of 10^{-6} s and expecting 10^5 time step calculations.

2.5 Simulation Configuration

Simulations are conducted on an $8ID \times 8ID \times 36ID$ ($x \times y \times z$) computational domain. Various domain sizes were tested to determine this domain width. The

width of the domain is set to $8ID$ (in x and y) as this are the smallest size tested when the vectors at the bounds of the domain have no fluctuation. The jet nozzle is modeled as a round vent with a radius of 2.6 mm and an inert surface with a radius of 4.5 mm, representing the wall thickness of the nozzle. Simulations are run with multiple meshes and mesh refinement. The coarsest case set 8 cells across the jet nozzle exit ($ID/\Delta x = 8$) and consisted of 36 meshes. Each mesh size is 16^3 . The medium and high resolution cases consist of 42 meshes; 16 meshes surrounding the jet core of resolutions of $ID/\Delta x = 16$ and 32 with grid coarsening (by a factor of 2). Meshes are load balanced to 32^3 and 64^3 grid points per mesh. These multi mesh and grid refinement strategy are adopted to allow for shorter run times. Fig. 2.8 shows the grid near the jet exit and Fig. 2.9 shows this mesh arrangement. Runtimes on the NIST HPCC Burn were 1.97 hrs, 7.45 hrs, and 61.52 hrs for the $ID/\Delta x = 8$, 16, and 32 resolution cases.

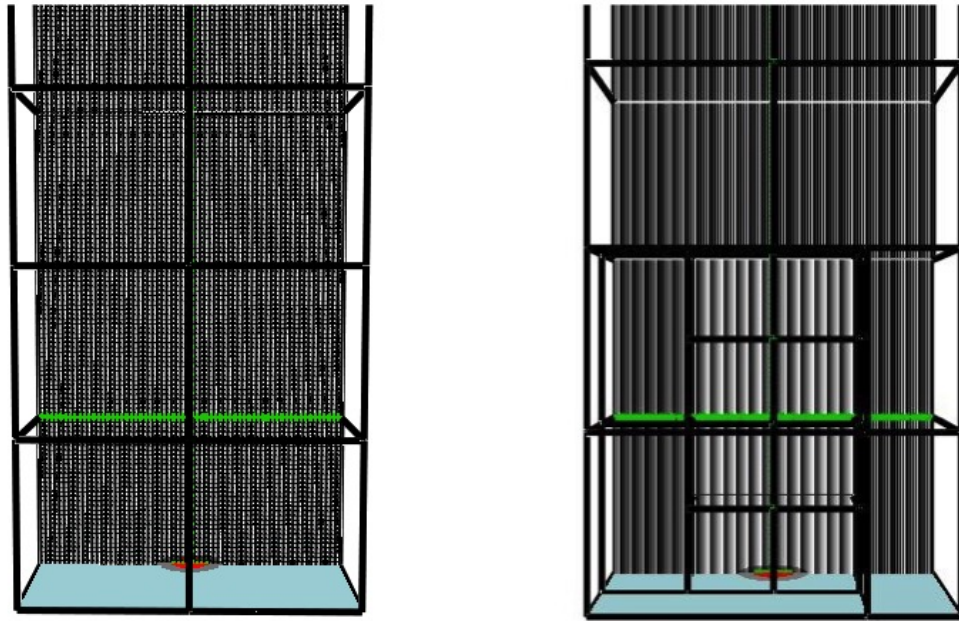


Figure 2.8: Smokeview renderings showing the mesh arrangement for the simulation with a resolution of $ID/\Delta x = 8$ (left) and $ID/\Delta x = 16$ and 32 (right).

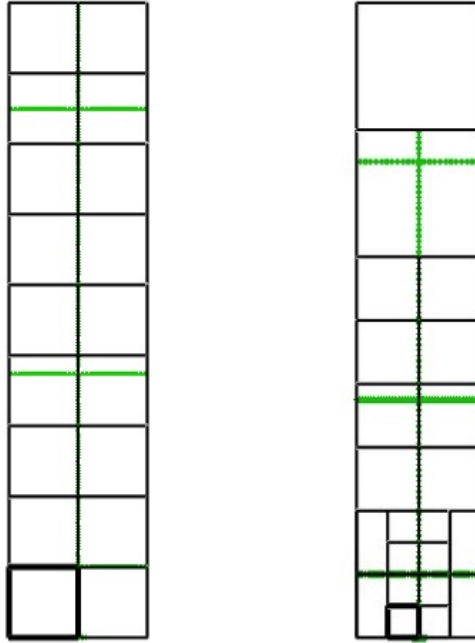


Figure 2.9: Smokeview renderings showing the mesh arrangement for the simulation with a resolutions of $ID/\Delta x = 8$ (left) and $ID/\Delta x = 16$ and 32 (right) These are 2D representations of the computational domain. The dark lines indicate mesh boundaries and the green points are the location of the devices. (Left) The mesh arrangement for the courses resolution case is 36 uniform meshes with a mesh size of 16^3 . (Right) The mesh arrangement for the medium and finest resolution simulation. Due to restrictions in computing power, a non uniform grid had to be applied. The region surrounding the jet exit has the resolution specified by $ID/\Delta x = 16$ and 32 . The surrounding meshes are coarsened by a factor of two with the top two meshes being coarsened again by a factor of 2.

The jet nozzle was modeled as a radial vent with a radial inert surface centered under the vent. The radius of the vent and inert surface were set to 5.2 mm and 9.0 mm, respectively. Fig. 2.10 shows the nozzle and device arrangement. Being a structured, cartesian grid, FDS is limited in its ability to model circular vents. A weighting factor is assigned to each cell that is determined to be a vent cell so that the mass flux through the vent is conserved.

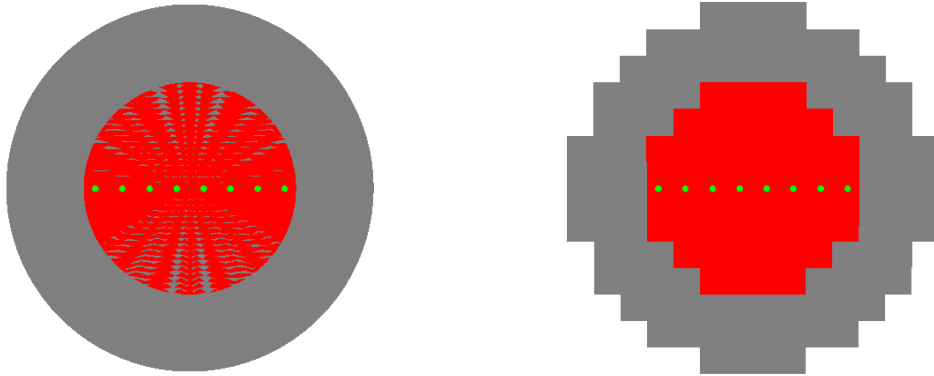


Figure 2.10: (Left) Smokeview rendering of the simulated jet nozzle and device configuration for the $ID/\Delta x = 8$ case. Devices were placed in each grid cell across the vent opening. (Right) FDS snapped nozzle configuration.

2.6 Boundary Conditions

Wall boundaries were specified as Dirichelt boundary condition; the coflow velocity was set to the value of 9.2 m/s.

Various test simulations were run to establish the inlet boundary conditions for the jet. Initially, the jet was given a flat velocity profile where the specified velocity was the cited centerline value or $1.28u_{bulk}$ [9]. This boundary condition did a poor

job of capturing the jet profile. The parabolic profile was also tested. Application of a parabolic profile with the updated code yielded magnitudes of velocity that were twice the experimental values and a narrower plume profile. Appendix A presents the test simulation results of the various inlet condition tests.

To most accurately capture the flow characteristics of a turbulent flow in a pipe, a new profile was created:

$$u(r) = \begin{cases} u_0 & 0 \leq r < R - \delta \\ u_0(1 - \frac{(r-R+\delta)^2}{\delta^2}) & R - \delta \leq r \leq R \end{cases} \quad (2.4)$$

so that $\frac{du}{dr} = 0$ in the center of the flow and decays parabolically so $u = 0$ at the pipe wall. Fig. 2.11 shows this profile. This boundary layer thickness δ , or the displacement thickness, is calculated so that

$$\frac{\int_0^{2\pi} \int_0^R u(r) r dr d\theta}{\int_0^{2\pi} \int_0^R r dr d\theta} = u_{bulk} \quad (2.5)$$

or, expanded

$$\frac{\int_0^{2\pi} \int_0^{R-\delta} u_0 r dr d\theta + \int_0^{2\pi} \int_{R-\delta}^R u_0 [1 - \frac{(r-R+\delta)^2}{\delta^2}] r dr d\theta}{\int_0^{2\pi} \int_0^R r dr d\theta} = u_{bulk} \quad (2.6)$$

This was added to the user inputs of FDS where 'boundary layer' can be specified for a surface when a radius is specified for the corresponding vent. The maximum velocity, bulk velocity and displacement thickness are the quantities that characterize the flow. Two of the three input quantities must be specified by the user. FDS will calculate the third to preserve the mass flux through the vent. The maximum velocity and bulk velocity were specified for each of the simulations.

While testing jet boundary conditions, Constant Smagorinsky, Dynamic Smagorinsky, Vreman, and Deardorff turbulence models were tested. During testing, no

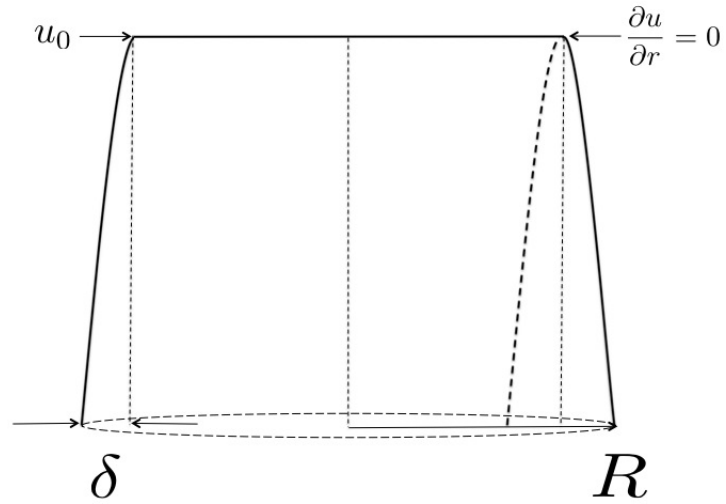


Figure 2.11: Boundary layer profile.

appreciable difference was noted; therefore, the default (Deardorff) model is used as it is the most efficient computationally. Tests were also conducted with the introduction of turbulence at the boundary. FDS uses the synthetic eddy method (SME) put forth by Jarrin [18]. Various fluctuation velocities, quantities and sizes of eddies were tested. This turbulence was effective at low resolution, but produced poorer results. These results can be seen in Appendix A.

Chapter 3: Results and Discussion

3.1 General Information

After completing all three simulations, the results are compared to experimental observations using a qualitative description of the flow. Various profiles and turbulence models are considered when establishing the velocity boundary conditions at $z/ID = 4$. Based on these models, velocity profiles at various axial positions above the nozzle are presented here and results from different mesh sizes are compared. Additionally, scalar mean and fluctuating quantities are compared to experimental data. The simulations in this study are performed on the Linux cluster (Burn) at the NIST campus in Gaithersburg, MD. FDS subversion 22231 is used to run the simulations. Matlab R2102b is used to post process and plot data.

3.2 Inlet Boundary Conditions

As described in Chapter 2, a new profile for the jet inflow velocity boundary condition was created. This profile was confirmed by placing a boundary device in each of the cells at the boundary. Fig. 2.10 shows the device and grid arrangement at the nozzle for the $ID/\Delta x = 8$ case. Fig. 3.1 shows the expected vs. output velocity

profile at the jet exit. As the devices measured velocity at the center of the top face, the velocities and the radial coordinates are measured at $\Delta y/2$. Velocity errors at the boundary are 10^{-14} m/s in all of the cases. The velocities and positions are corrected by $r = \sqrt{x^2 + \frac{\Delta y^2}{2}}$ where $\Delta y = \Delta$. Confirmation that propane is issued into the domain is shown in Fig. 3.2.

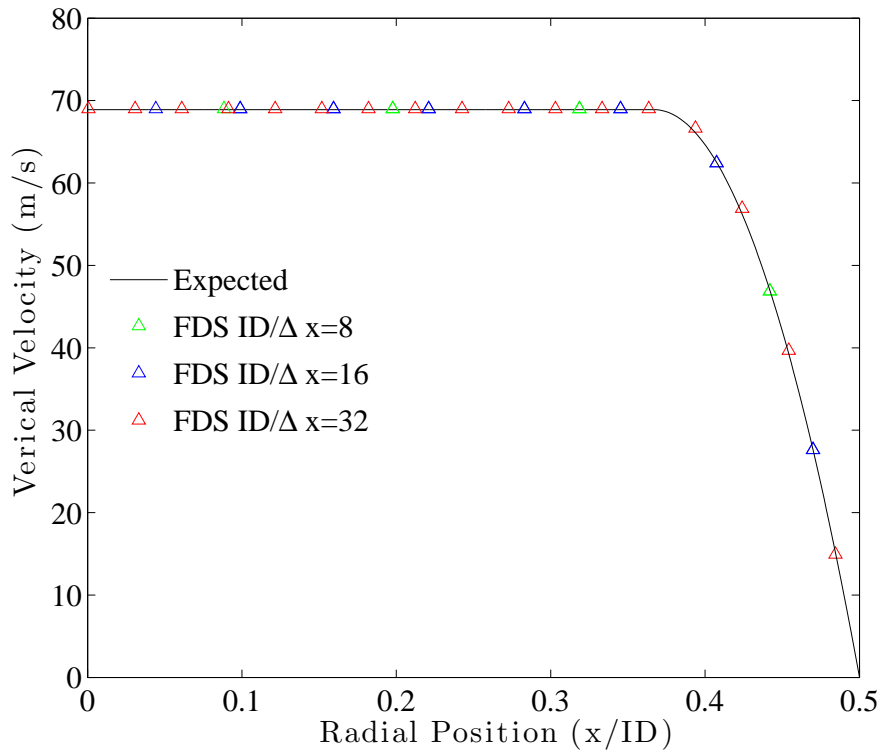


Figure 3.1: FDS output velocity profile at the jet exit, for resolutions of $ID/\Delta x = 8, 16,$ and $32,$ against the expected exit velocity profile.

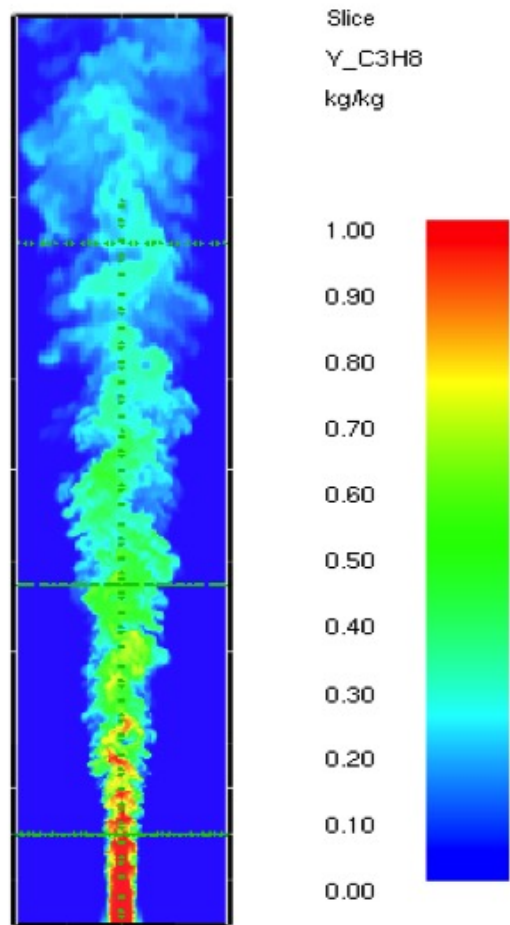


Figure 3.2: Smokeview slice file of mass fraction of propane. Propane is being issued into the domain with a mass fraction of 1.

3.3 Centerline Profiles

Fig. 3.3 presents the centerline profiles of vertical velocity and mixture fraction against experimental results. A grid resolution of $ID/\Delta x = 8$ under predicts vertical velocities at the jet exit and appears to maintain a potential core further down field, resulting in a significant over prediction of the centerline velocity in the mid field. This resolution better predicts centerline velocities in the far field; this is partially due to plume expansion downstream. At a downstream location of $z/ID = 30$, the jet plume is approximately four times wider, making the resolution of the plume four times greater.

At resolutions of $ID/\Delta x = 16$ and 32 , there is a noticeable drop in the vertical velocity which occurs in the first two to three cells downstream of the jet nozzle. The potential core of the jet in these initial cells breaks down and then re-stabilizes, as evidenced by the near zero slope between $z/ID = 2$ and 7 . The far field velocities are grid converged. For further analysis of this issue, it is recommended that another simulation with higher resolution is run to check for grid convergence. The initial drop in velocity at the jet exit may be minimized at a higher resolution, particularly when the boundary layer of the jet is well resolved.

Fig. 3.4 shows a semilog plot of the centerline vertical velocities and mixture fraction. The $ID/\Delta x = 8$ simulation predicts minimal velocity and mixture fraction decay until 15 diameters downstream where the higher resolutions predict decay between 7 and 10 diameters downstream. In all three cases, FDS predicts a faster decay of the centerline velocity. Although FDS over predicts the mixture fraction

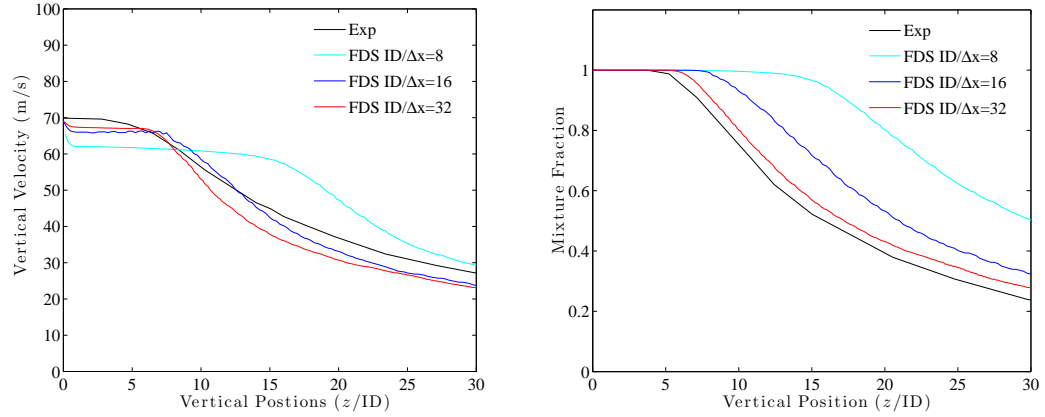


Figure 3.3: FDS predictions of centerline mean vertical velocity and mixture fraction for the Sandia nonpremixed, nonreacting propane jet. Results are shown for $ID/\Delta x = 8, 16,$ and 32 grid resolutions.

of propane downstream, the prediction of centerline mixture fraction decay, for the tested resolutions, seem to reflect experimental decay.

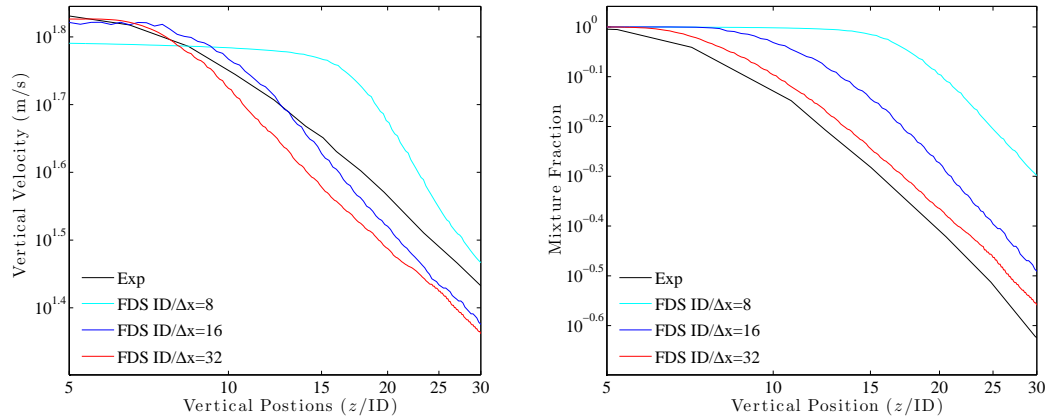


Figure 3.4: FDS predictions of centerline mean vertical velocity and mixture fraction decay for the Sandia nonpremixed, nonreacting propane jet. Results are shown for $ID/\Delta x = 8, 16,$ and 32 grid resolutions.

3.4 Radial Profiles

Fig. 3.5 presents FDS simulated vertical, radial, and mixture fraction mean and rms quantities against experimental values at a location of $z/ID = 4$. Results for mean vertical velocities are symmetric and mean radial velocities are antisymmetric. Peak mean vertical and rms velocities properly correlate with experimental values. The profile of the mean vertical velocity indicates slower simulated expansion of the plume. This is evidenced in the radial velocity profile where the predicted velocities within the jet nozzle are lower (in magnitude) than the jet and air seeded experimental data. The mean mixture fraction simulation results echo the results of the mean vertical and radial velocity profiles, where the simulation results predict a sharp gradient at the shear layer. Rms mixture fraction predictions are poor as there is a sharp spike in fluctuations in the shear layer. Qualitatively, these results are similar to results of mass fraction rms predictions of the Sandia helium pool fires in the FDS Validation Guide [19].

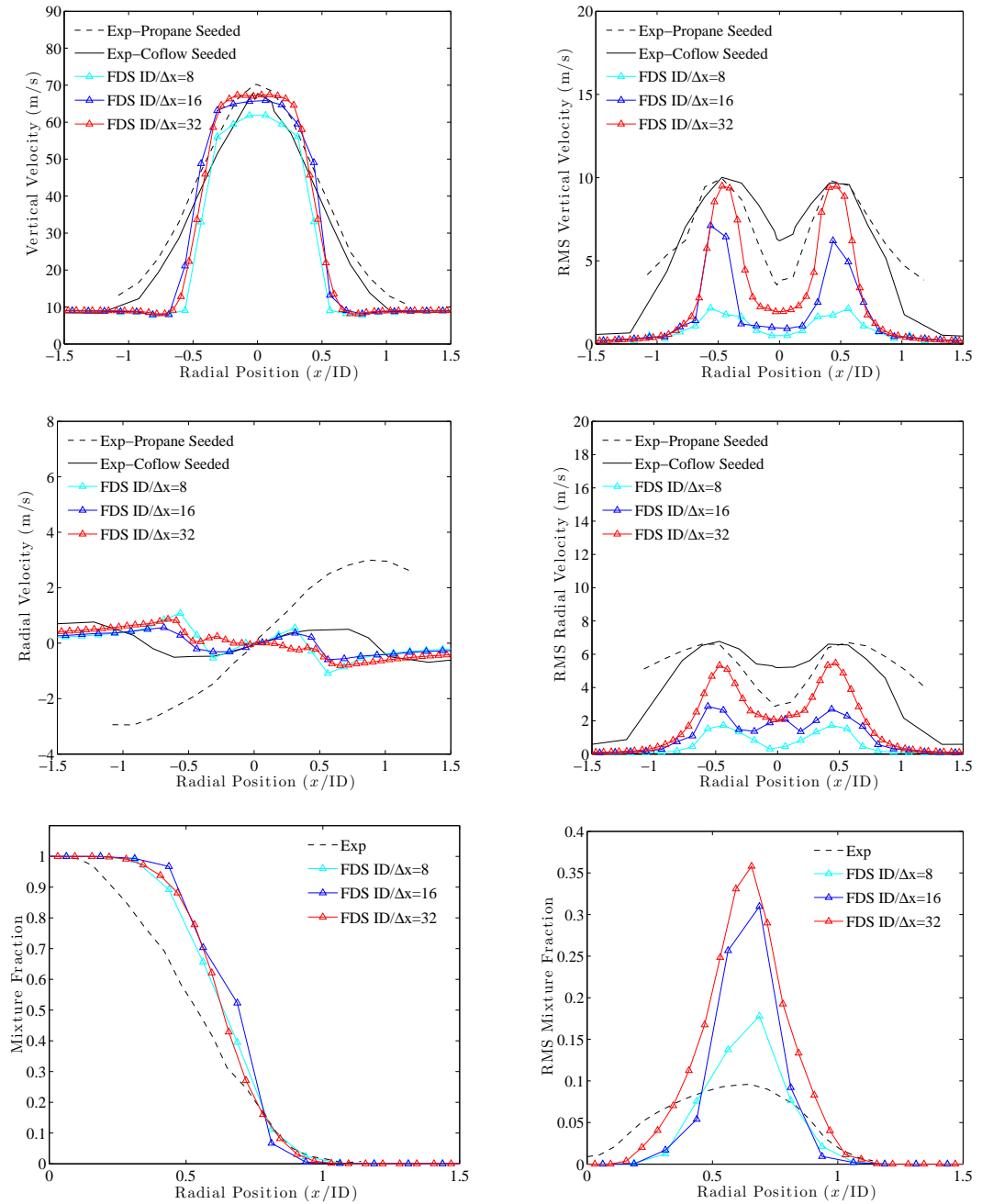


Figure 3.5: FDS predictions of mean and rms vertical and radial velocity profiles and mean and rms mixture fraction for the Sandia nonpremixed, nonreacting propane jet at the location $z/ID = 4$ above the jet nozzle. Results are shown for $ID/\Delta x = 8, 16,$ and 32 grid resolutions.

The jet plume at a location of $z/ID = 15$ is approximately 3D. Coarse resolution results indicate that the simulated potential core is intact; the peak mean vertical velocity profile shows a narrow profile with a centerline velocity that is 20 m/s greater than experimental results. Mean radial velocities are antisymmetric with flow direction that is opposite to experimental results. Coflow air is entraining, the plume expansion is under predicted. At higher resolutions, mean and fluctuating quantities have closer resemblance to experimental data. Mean radial velocities, at a resolution of $ID/\Delta x = 32$ are predicting the correct direction. Both mean and rms radial velocity magnitudes are under predicted. Mean mixture fraction predictions, at a high resolution, are in proper agreement with experimental results.

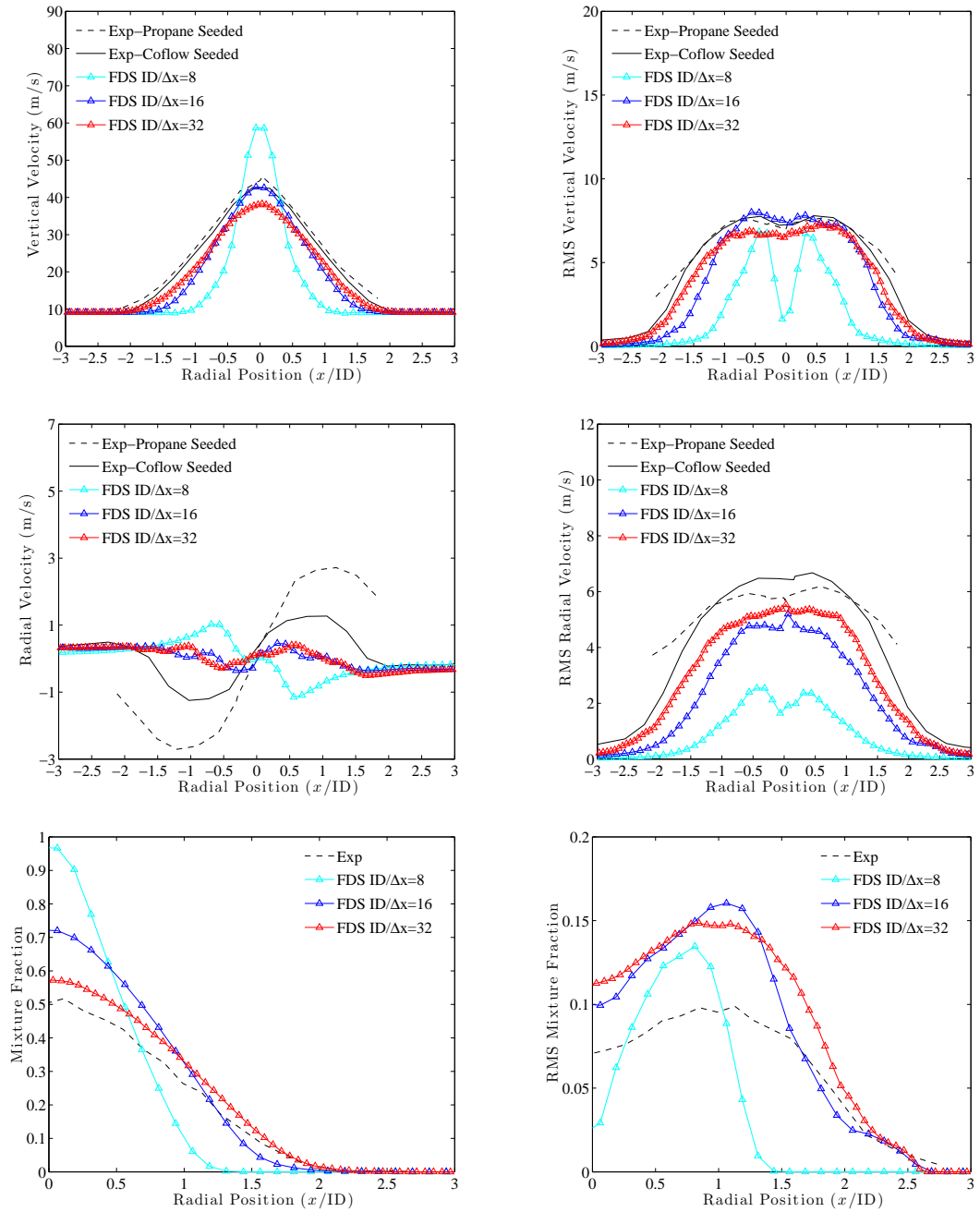


Figure 3.6: FDS predictions of mean and rms vertical and radial velocity profiles and mean and rms mixture fraction for the Sandia nonpremixed, nonreacting propane jet at the location $z/ID = 15$ above the jet nozzle. Results are shown for $ID/\Delta x = 8, 16,$ and 32 grid resolutions.

At an elevation of $z/\text{ID} = 30$, the jet plume is approximately $7D$ wide. This is close to the total width of the domain. During preliminary testing, the domain width was determined and assessed solely on the mean vertical velocity. As seen in Fig. 3.7, mean vertical velocities at the boundaries are the coflow velocity and the fluctuations at the boundaries are zero. The close boundary can cause issues in the simulated velocity fields as the plume might intermittently interact with the boundary; with Dirichlet conditions at the boundary, there would be tendencies towards the set value. With more time and computational resources, a larger domain could be created. At this elevation, there are 16, 32 and 64 cell resolutions of the plume. There is minimal difference in results between cases of jet nozzle resolution of $\text{ID}/\Delta x = 16$ and 32. These results are converged and indicate that a resolution of $\text{ID}/\Delta x = 32$ may be converged at $z/\text{ID} = 4$ and 15, although it is apparent that the finest resolution case does not resolve the potential core at a distance z/ID above the jet nozzle.

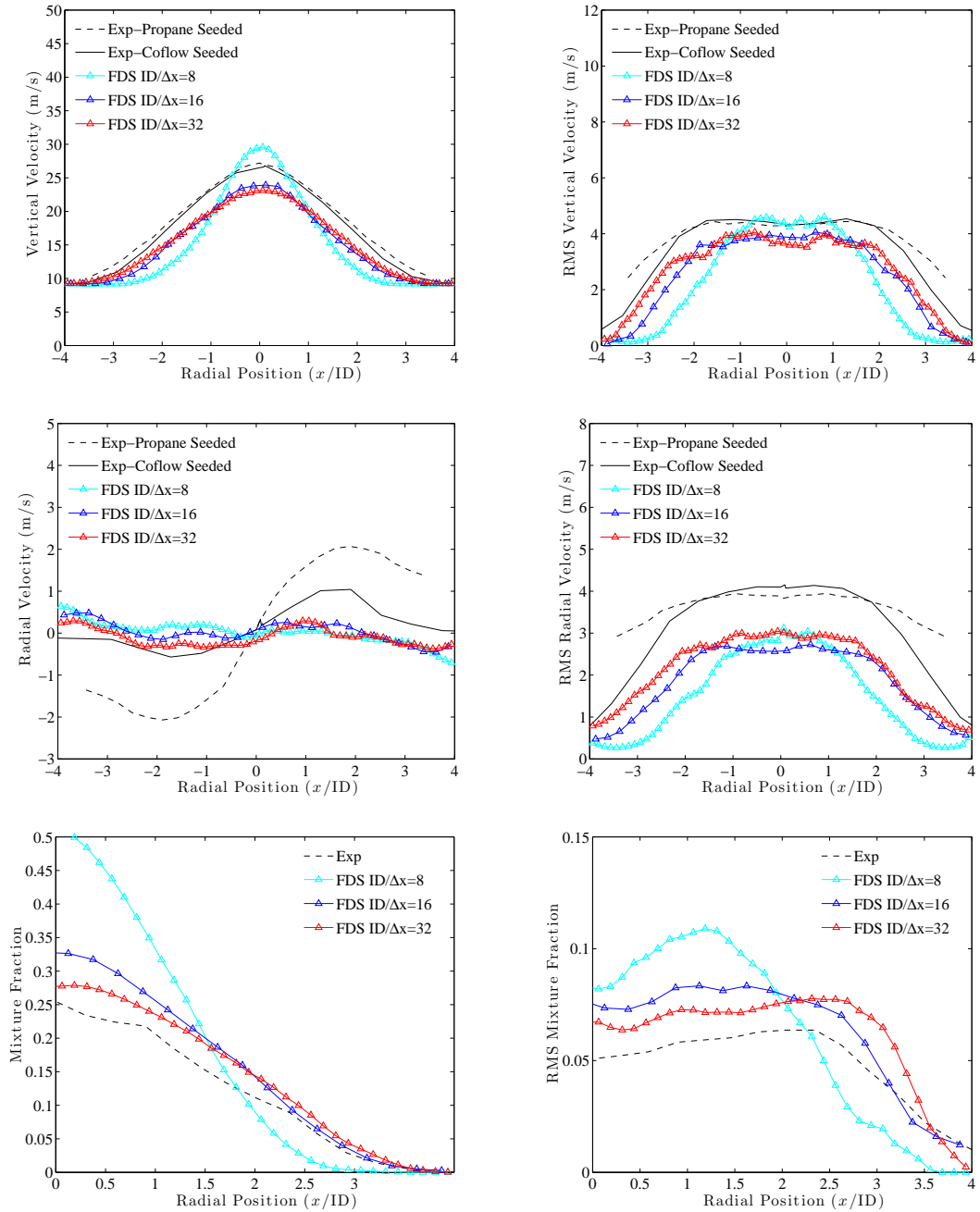


Figure 3.7: FDS predictions of mean and rms vertical and radial velocity profiles and mean and rms mixture fraction for the Sandia nonpremixed, nonreacting propane jet at the location $z/ID = 30$ above the jet nozzle. Results are shown for $ID/\Delta x = 8, 16,$ and 32 grid resolutions.

3.5 Statistical Convergence

The time step for the $ID/\Delta x = 8, 16$ and 32 are 0.402×10^{-5} s, 0.201×10^{-5} s, and 0.100×10^{-5} s respectively. Fig. 3.8 shows device outputs at elevations of $z/ID = 4, 15$ and 30 , for the $ID/\Delta x = 32$ case. These devices are at a radial location of $0.5R$. Mean and rms are presented to show that the quantities of interest are converged. Rms values are calculated by

$$w_{rms} = \sqrt{\frac{1}{N} \sum_{n=1}^N (\bar{w} - \bar{w})^2} \quad (3.1)$$

As seen in Figs. 3.5-3.7, these mean and rms values correlate with the output from the FDS line devices.

3.6 Filtered Considerations

Experimental and FDS quantities are not explicitly the same values. The exact filtering of the experimental values are not disclosed. In general, velocities (u) are described as a mean and fluctuating quantity ($\bar{u} + u'$) [20]. Mean quantities of velocity can be expressed

$$\langle \bar{u} + u' \rangle = \langle \bar{u} \rangle + \langle u' \rangle \quad (3.2)$$

where $\langle u' \rangle$ can be approximated as $\langle \bar{u}' \rangle$. FDS calculates velocity fluctuations using subgrid kinetic energy

$$\langle \bar{u}' \rangle = \sqrt{\frac{2}{3} k_{sgs}} \quad (3.3)$$

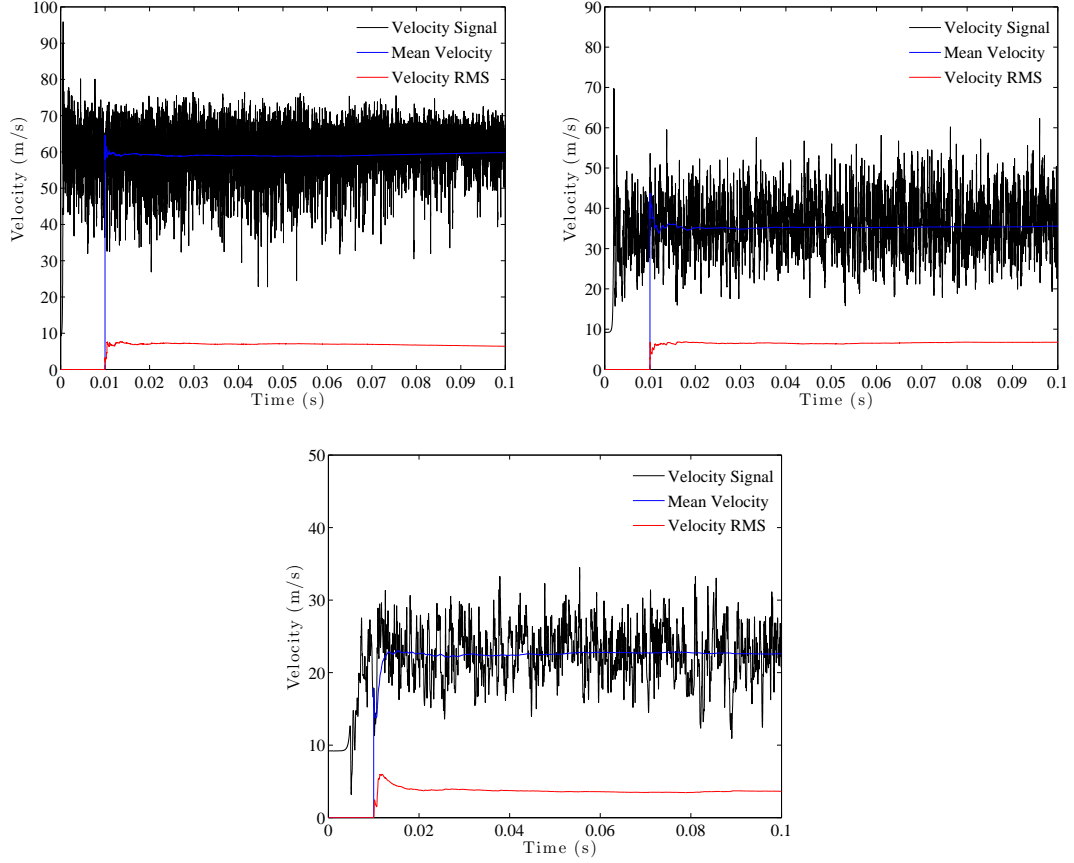


Figure 3.8: Vertical velocity signals at elevations of $z/ID = 4, 15$ and 30 at a radial location of $0.5R$. Results are shown for $ID/\Delta x = 32$. Mean and rms are presented to show that the quantities of interest are converged.

where the subgrid kinetic energy is calculated by the turbulent viscosity [8]

$$k_{sgs} = \left(\frac{\mu_t}{C_\nu \rho}\right)^2 \quad (3.4)$$

Fig. 3.9 shows the above correction where the fluctuation and mean velocities are considered. This correction provides a slight shift toward higher velocity values. This definition of a filtered mean value and fluctuation could only be made for filtered velocity values. A practical correction could not be applied to the fluctuation results or the mixture fraction information; therefore, this correction is not applied

to the final analysis of these simulation results.

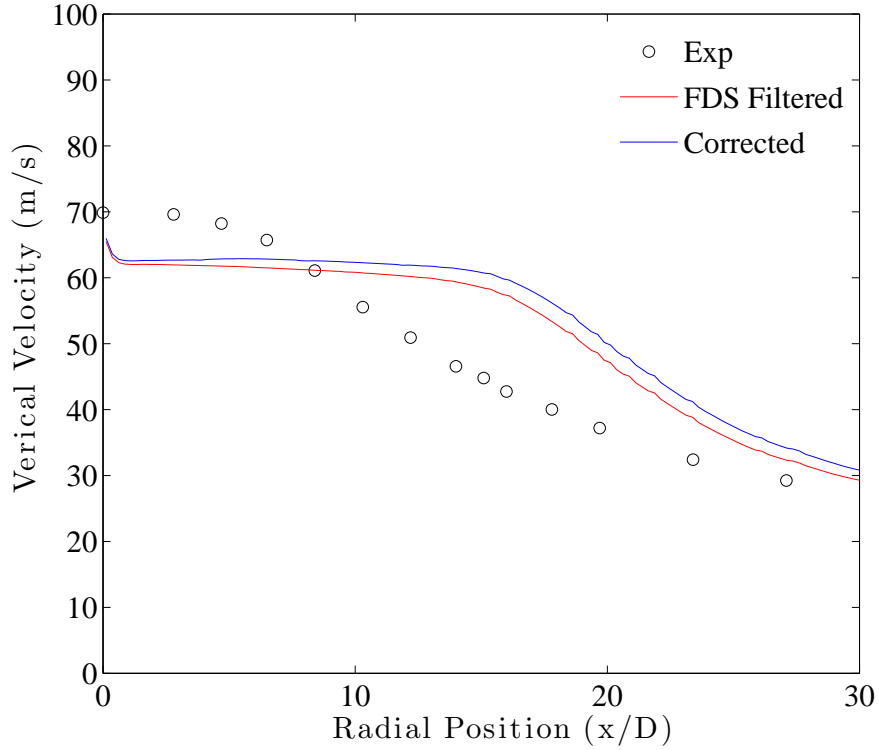


Figure 3.9: FDS prediction and corrected of centerline mean vertical velocity for the Sandia nonpremixed, nonreacting propane jet. Results are shown for $ID/\Delta x = 32$ grid resolution.

3.7 Profile Error

Multiple test simulations are run to identify the best matching jet velocity boundary conditions. During testing of the parabolic inlet velocity profile, it was noted that there was a distinctive double hump in \bar{w} at $z/ID = 4$ location. Upon further inspection, when a mesh boundary split the vent, each half of the event calculated a separate, independent parabolic velocity profile. Fig. 3.10 shows

a Smokeview visualization of this issue. This bug inhibits FDS ability to properly reflect the parabolic velocity profile, rendering the simulation ineffective; this issue was corrected in the FDS code.

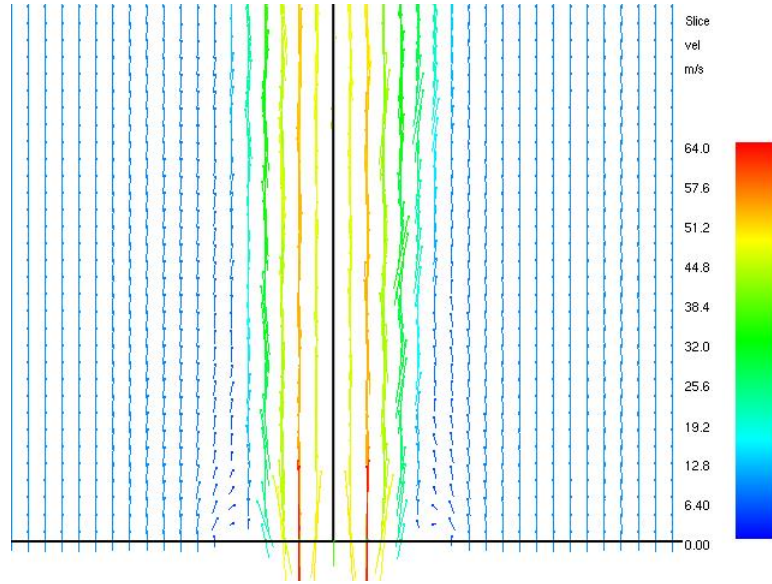


Figure 3.10: Smokeview rendering showing a velocity profile error when a parabolic profile is assigned to a vent that spans two meshes. FDS created two parabolic profiles on either side of the mesh boundary

3.8 Vorticity at the Boundary

Fig. 3.11 shows a Smokeview rendering of a slice of velocity where there is artificial entrainment of momentum at the boundaries. In the cases run, FDS calculated Dirichlet boundary conditions by assigning the boundary cell velocity to the adjacent ghost cell. FDS was assigning this boundary cell velocity by default. In response to this issue, a new method of calculating Dirichlet boundary conditions

was created. The new method of calculating boundary conditions sets the tangential ghost cell velocity to the far field velocity. In the cases run, this alteration to FDS guarantees zero numerical vorticity at the boundaries, see Fig. 3.12.

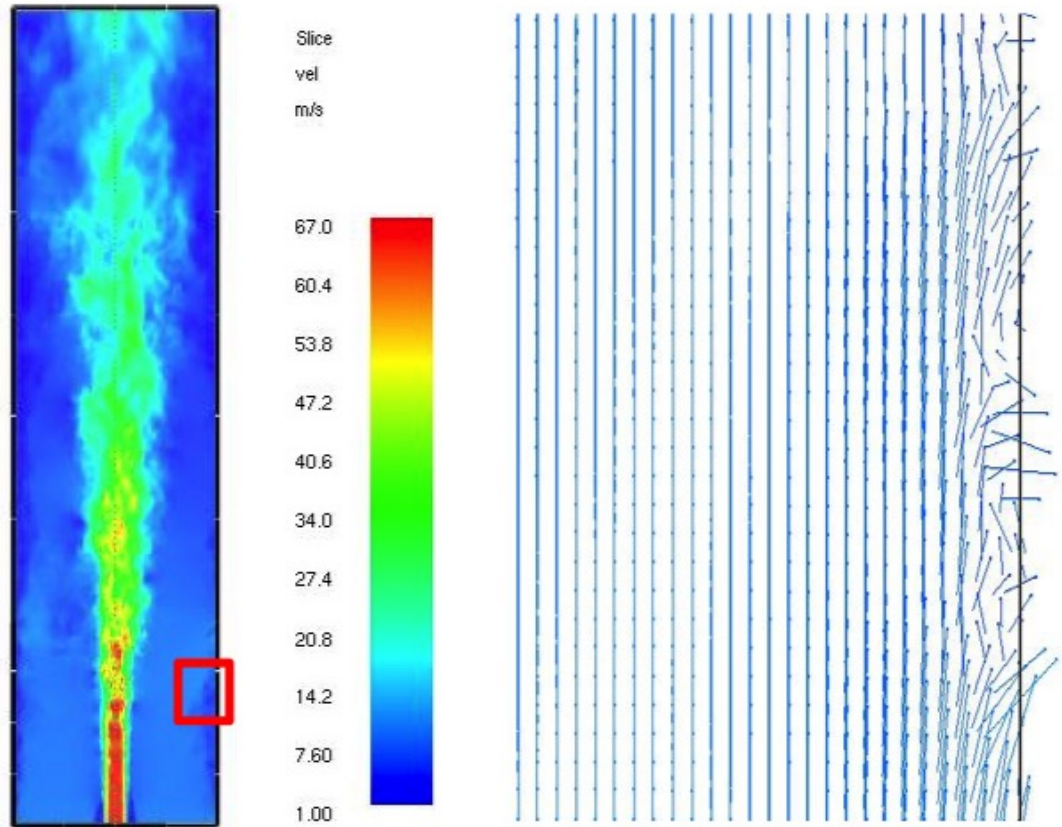
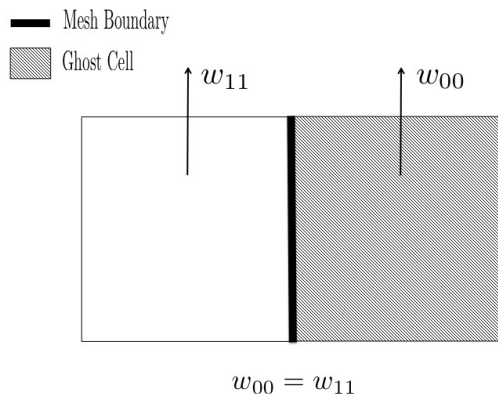


Figure 3.11: (Left) Smokeview rendering showing a slice of velocity - note the artificial flow perturbations at the boundaries. (Right) A close up rendering of Smokeview multi-vector slice of velocity.

Default 'Open' Boundary Condition



New 'Open' Boundary Conditions

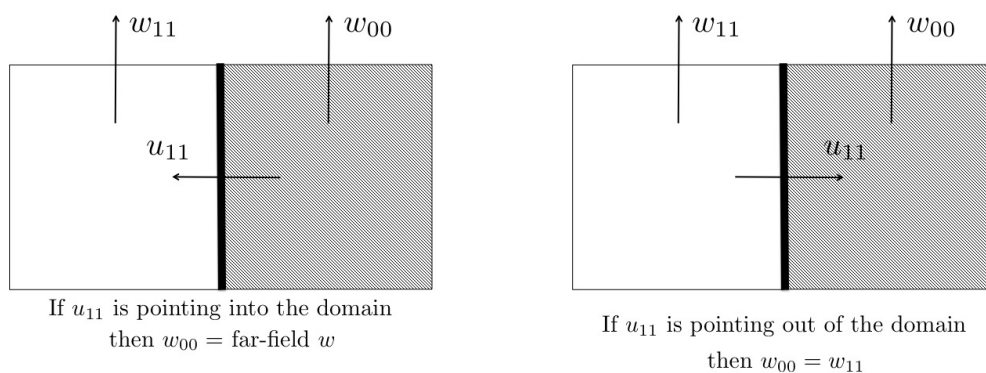


Figure 3.12: (Top) Old method of calculating 'Open' boundary condition whereby the ghost cell tangential velocity is set by the adjacent cell. (Bottom) New method of calculating 'Open' boundary conditions by setting the tangential ghost cell velocity is set to the far field velocity if flow is into the domain or the ghost cell tangential velocity is to the adjacent cell.

3.9 Viscosity at Mesh Boundaries

While trouble shooting the inlet boundary conditions, an error with the viscosity calculated at mesh boundaries was discovered. Fig. 3.13 shows a slice of viscosity from a Smokeview output. At mesh boundaries, a ghost cell was not being populated with the appropriate velocity value. Fig. 3.14 shows an arrangement of cells near a mesh boundary. At mesh boundaries, the first cell in the domain is reliant on its nine surrounding cells. If looking at cell u_{11} , the cell at the cruciform joint, ghost cell u_{00} , was not being populated with the correct velocity; when surrounding cells are used to calculate an average velocity for cell u_{11} , a value of 0 was being averaged due to cell u_{00} . The result was a lower viscosity value of the cell at the mesh boundary. In preparation for the release of FDS 6.2, the entire FDS validation suite was run with this correction. For the first time since FDS's inception, the entire validation suite ran to completion without errors due to numerical instabilities.

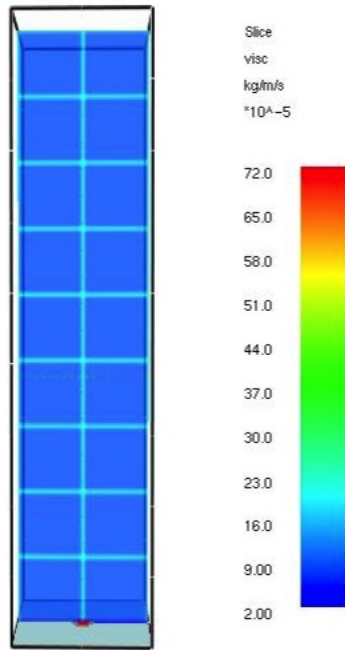


Figure 3.13: Smokeview rendering showing FDS incorrectly calculating the viscosity at mesh boundaries.

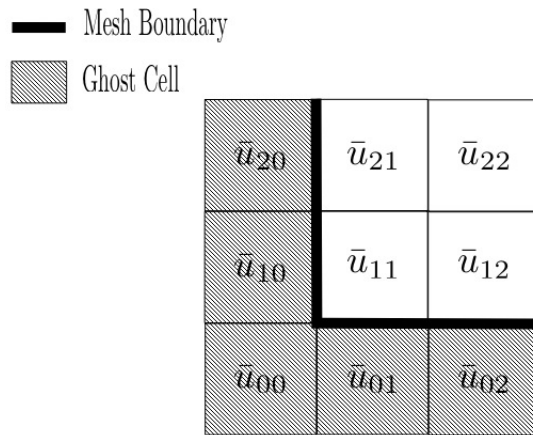


Figure 3.14: While populating cell u_{11} , ghost cell u_{00} was not being populated causing a value of 0 to be averaged at the mesh boundary.

Chapter 4: Conclusion

Simulations of a turbulent momentum driven jet were carried out in FDS. These simulations challenged the capabilities of FDS and identified strengths and weaknesses. This research discovered and corrected various bugs in FDS including a parabolic velocity profile error, viscosity calculations at mesh boundaries and introductions of numerical vorticity at open boundaries. Additionally, a new profile for jet inflow velocity boundary conditions was created. Simulation results proved that at resolutions of $ID/\Delta x = 32$, results are closer to experimental data, but a resolution of $ID/\Delta x = 16$ provided very similar results with a lower computational cost. Mean and fluctuation vertical velocities and mean mixture fraction profiles are well-captured; however, mixture fraction fluctuations are over predicted and mean vertical velocity predictions dropped cells above the nozzle . All the simulations conducted for this research will be incorporated into FDSs validation suite.

Future work should consist of:

1. Further exploration into the bug at the jet exit.
2. A grid sensitivity analysis of the near field flow to properly resolve the boundary layer of the flow.

3. A study on the effects of different turbulence models on far field predictions.

Appendix A: Contributions

Below provides a list of new user features and corrected bugs that were a direct result of the work conducted in this study. These features and fixes will be incorporated into newer release versions of FDS.

1. Correction of viscosity calculation at mesh boundaries
2. Correction of numerical instability at mesh boundaries in cylindrical calculations
3. Correction of parabolic velocity profile for a vent where a mesh boundary intersects the vent
4. Creation of a modified 'OPEN' boundary that sets tangential velocity components to far field values for inflow conditions and Neumann conditions for outflow conditions.
5. Creation of a plug flow with boundary layer velocity profile for radial vents
6. Creation of Mach number output quantities
7. Ability for devices to output non-dimensional lengths.

Appendix B: Testing Jet Boundary Conditions

B.1 Introduction

As described in the main text of this document, a large hurdle of this study is setting the jet inlet boundary condition. This appendix is to provide a small insight into the types of test simulations that were conducted while trying to set the jet boundary condition. The order of the presentation of these test results are not chronological and do not encompass all of the test simulations. Default FDS settings were used, unless otherwise stated. The majority of these tests were run before the corrections, mentioned in Chapter 3, were made. All of the plots in this appendix represent simulation data at an axial location of $z/ID = 4$.

B.2 2-Dimension Test Simulations

Fig. B.1 shows a 2D test where a parabolic velocity profile is used for the jet inlet condition. The specified velocity is 69 m/s, which is the observed centerline velocity. This figure shows the presence of the velocity profile error discussed in Chapter 3.

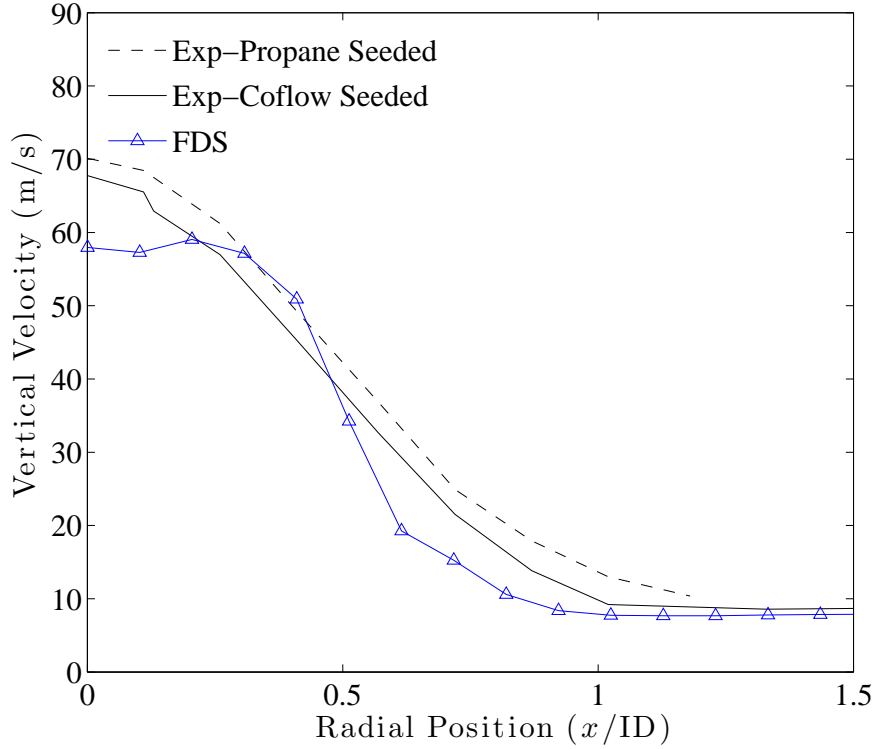


Figure B.1: A 2D simulation to test the jet boundary condition using a parabolic profile where the maximum velocity is specified as the observed maximum centerline velocity (69 m/s). Results show a grid resolution of $ID/\Delta x = 10$.

B.3 Axisymmetric Test Simulations

Fig. B.2 shows a bug while attempting a multimesh axisymmetric simulation. The Smokeview rendering is a slice of velocity magnitude; the black lines indicate mesh boundaries. The jet vent is located on the left most part of the domain. Artificial flow is created at the mesh boundaries causing numerical instabilities. The development team corrected this bug before running further axisymmetric calculations.

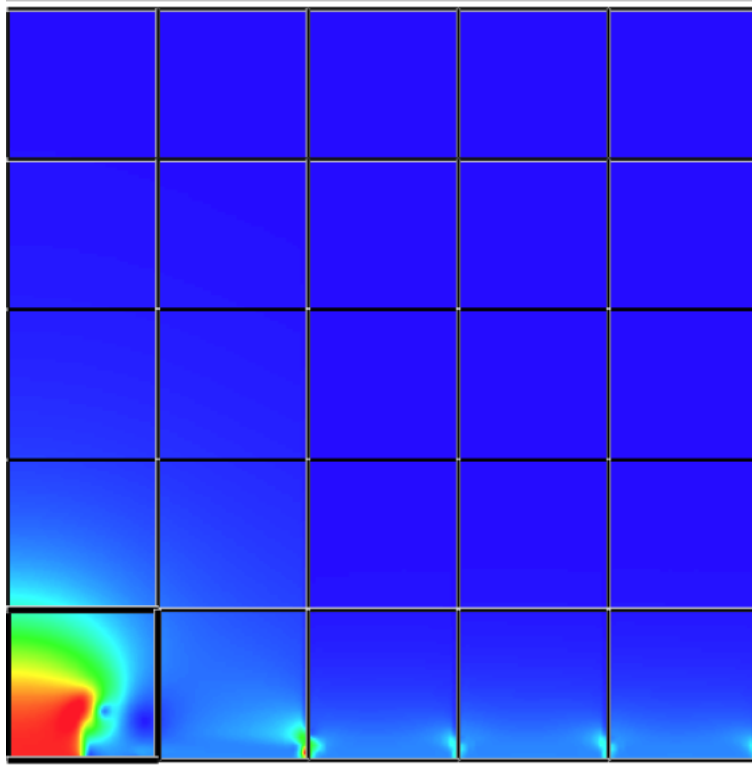


Figure B.2: A slice of velocity magnitude showing the presence of a bug while attempting a multimesh axisymmetric simulation. The black lines indicate mesh boundaries. The jet vent is located on the left most part of the domain. Artificial flow is created at the mesh boundaries causing numerical instabilities.

Fig. B.3-B.6 are samples of axisymmetric test cases. Fig. B.3 shows a test simulation using the experimental profile at $z/\text{ID} = 4$ and a specified centerline velocity of 69 m/s. The experimental profile at $z/\text{ID} = 4$ is tested as it is the first location where experimental data is known. As seen, at a resolution of $\text{ID}/\Delta x = 10$, the profile is under predicted. Fig. B.4 shows a test simulation using a parabolic profile and a specified centerline velocity of 69 m/s. As seen, at a resolution of $\text{ID}/\Delta x = 10$, the profile is under predicted. It is important to note that this simulation is run before fixing the parabolic profile bug discussed in Chapter 3. This a contributing factor to the under prediction of the centerline velocity.

Further exploration of the parabolic and experimental boundary conditions showed that mass at the boundary is not conserved. To conserve mass with a parabolic velocity profile

$$\frac{\int_0^{2\pi} \int_0^R u(r) r dr d\theta}{\int_0^{2\pi} \int_0^R r dr d\theta} = u_{bulk} \quad (\text{B.1})$$

where $u(r) = u_0 - \frac{u_0}{R^2} r^2$, then $u_0 = 2u_{bulk}$. Fig. B.5 shows axisymmetric simulation using a parabolic profile and a specified centerline velocity of $2u_{bulk}$. As seen, at a resolution of $\text{ID}/\Delta x = 8$, the profile is under predicted and at a resolution of $\text{ID}/\Delta x = 16$ the centerline is over predicted.

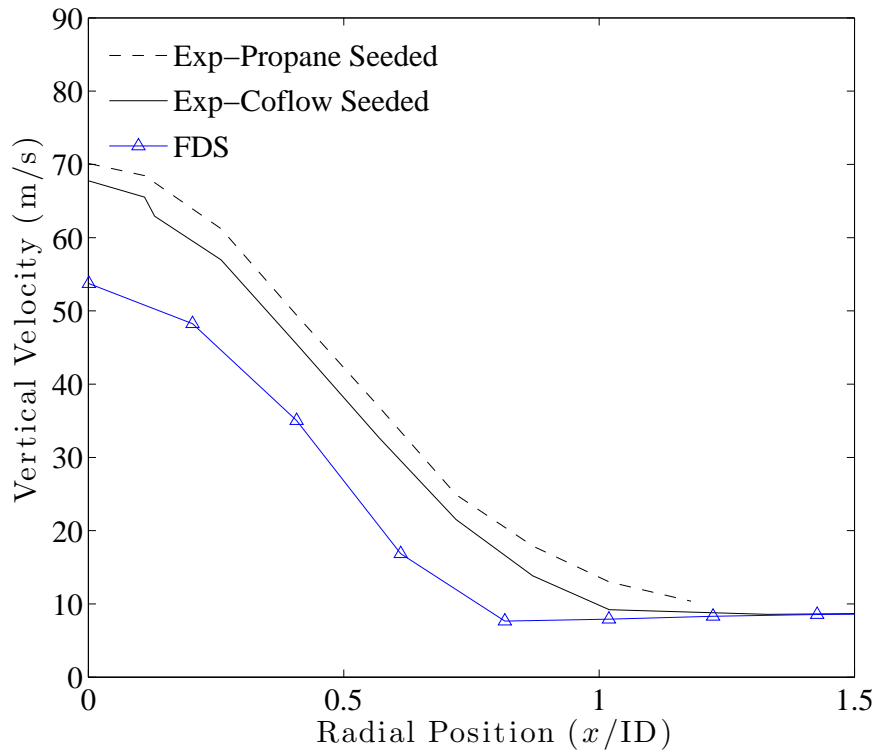


Figure B.3: Axisymmetric jet boundary condition test using the experimental profile at $z/ID = 4$ where the maximum velocity is specified as the observed maximum centerline velocity (69 m/s). Results show a grid resolution of $ID/\Delta x = 10$.

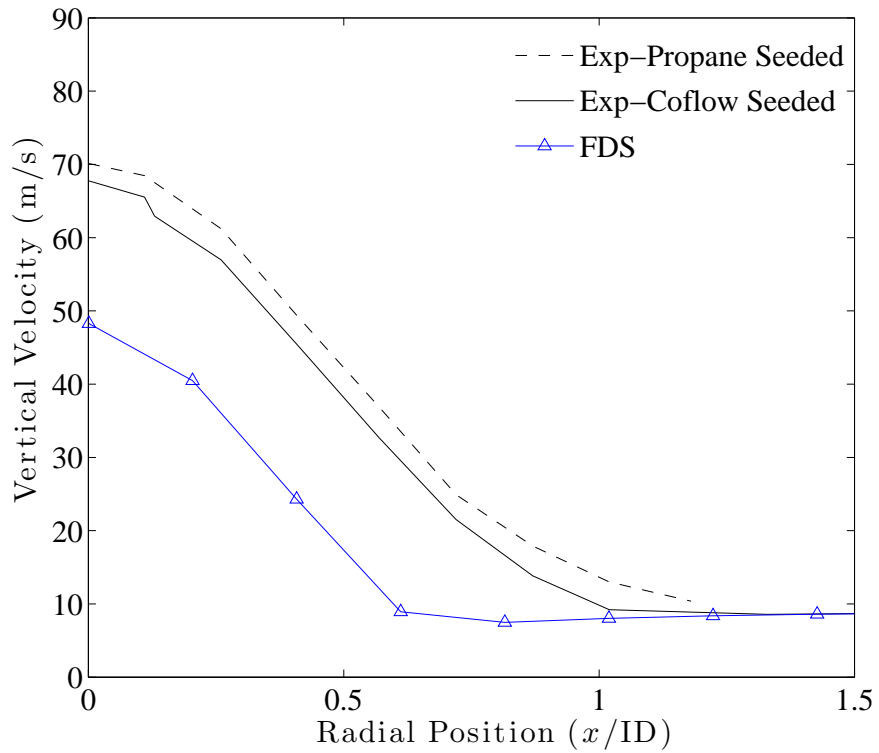


Figure B.4: Axisymmetric jet boundary condition test using a parabolic profile where the maximum velocity is specified as the observed maximum centerline velocity (69 m/s). Results show a grid resolution of $ID/\Delta x = 10$.

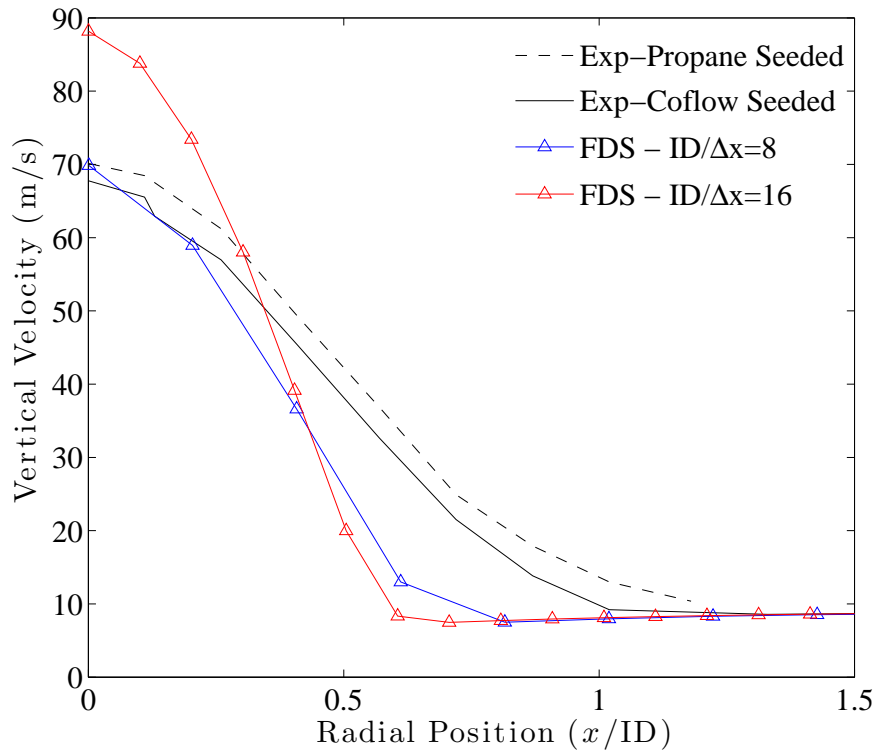


Figure B.5: An axisymmetric simulation to test the jet boundary condition using a parabolic profile where the centerline value is set to 106 m/s. Results show grid resolution of $ID/\Delta x = 8$ and 16.

Fig. B.6 shows an axisymmetric jet boundary condition test using a parabolic profile where the centerline velocity is specified as $2u_{bulk}$. This is a DNS simulation where the transport coefficients were set so that simulation results matched the experimental profile; viscosity is set to 5×10^{-3} kg/(m s) and the molecular diffusivity is 1×10^{-3} m²/s. Results show grid resolution of $ID/\Delta x = 20$. After this test, the parabolic profile bug is fixed and a new velocity profile is explored.

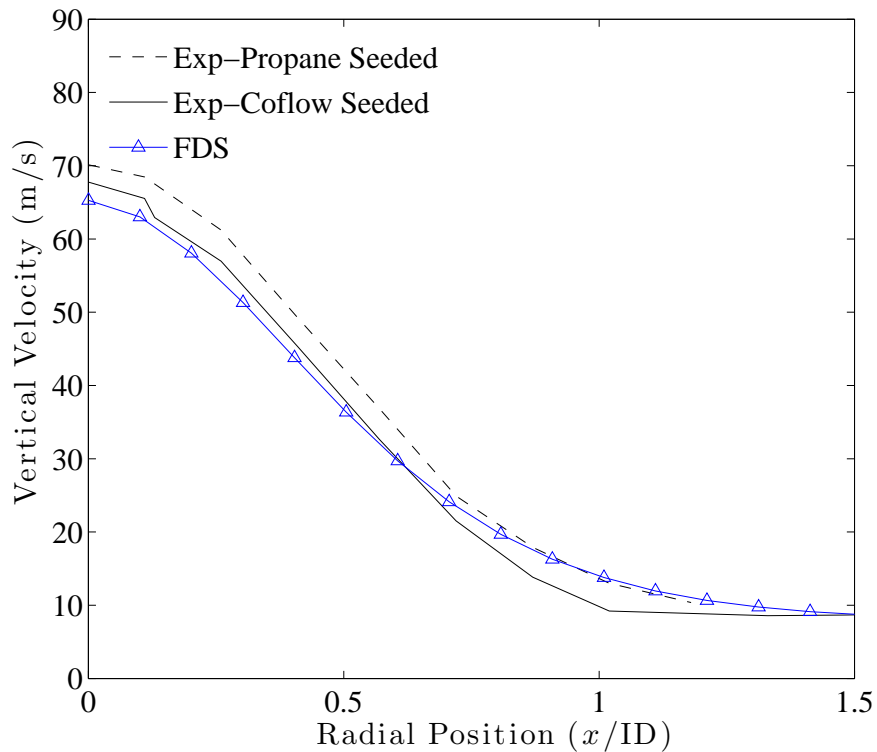


Figure B.6: An axisymmetric jet boundary condition test using a parabolic profile where the centerline velocity is specified as $2u_{bulk}$. This is a DNS simulation where the transport coefficients were set so that simulation results matched the experimental profile. Results show grid resolution of $ID/\Delta x = 20$.

B.4 3-Dimension Test Simulations

Fig. B.7-B.18 are samples of 3-Dimension test simulation results. Fig. B.7 shows a test simulation where the jet boundary condition test is specified as a mass flux; the experimental mass flux is used. Results show a grid resolution of $ID/\Delta x = 10$. The peak centerline vertical and peak fluctuations velocities were under predicted. Fig. B.8 and Fig. B.9 show simulations with a flat velocity profile where the velocities are specified at 53 m/s and 69 m/s. The flat profiles do not properly capture the shape of the mean or fluctuating velocity profile nor does it result in the proper prediction of the peak quantities. Also, as noted above, using a flat velocity profile of 69 m/s does not match experimental mass flux values.

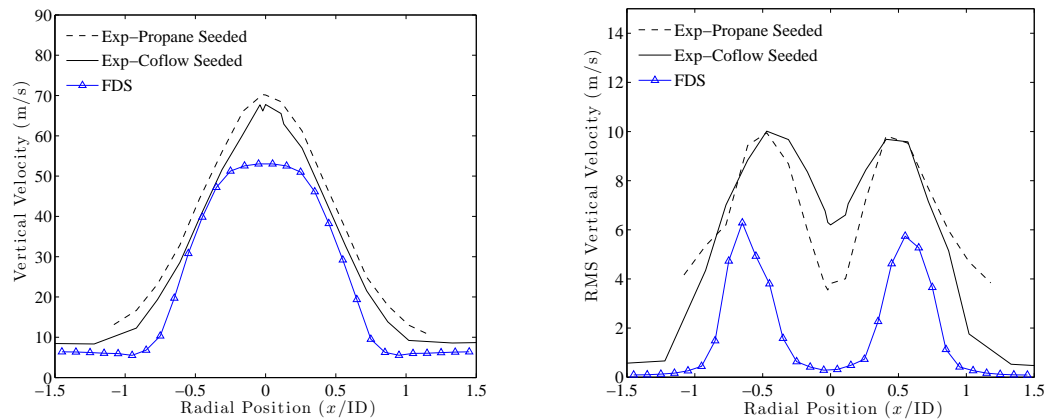


Figure B.7: Jet boundary condition test using the experimental mass flux at the boundaries. Results show a grid resolution of $ID/\Delta x = 10$. FDS currently only allows a flat mass flux profile.

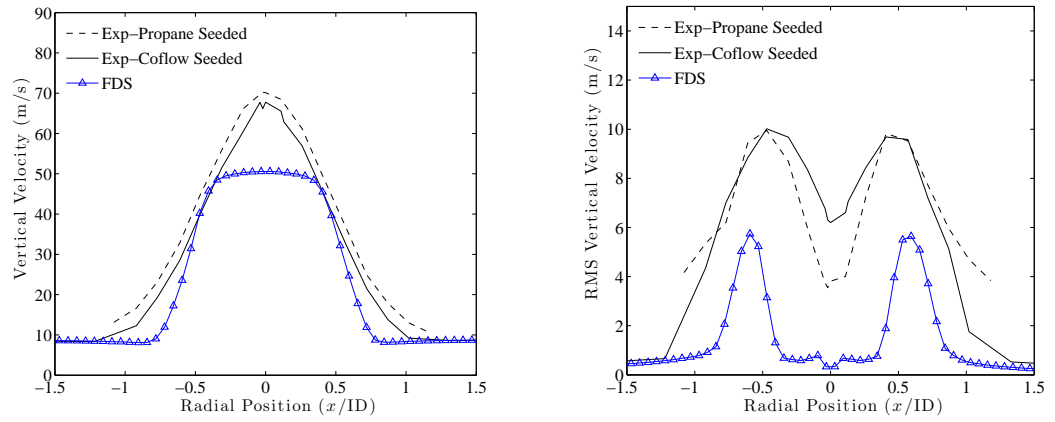


Figure B.8: Jet boundary condition test using a flat profile with a specified velocity of 53 m/s. Results show a grid resolution of $ID/\Delta x = 16$.

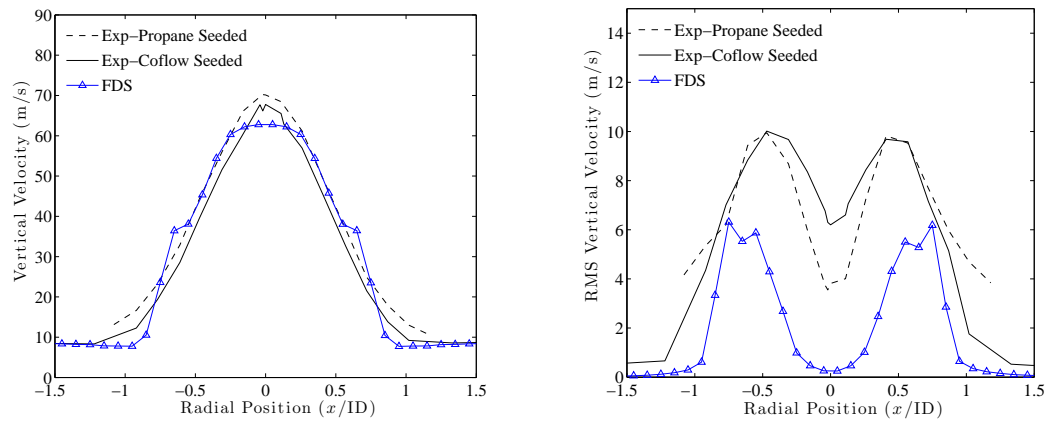


Figure B.9: Jet boundary condition test using a flat profile with a specified velocity of 69 m/s. Results show a grid resolution of $ID/\Delta x = 10$.

Fig. B.10 shows a comparison of simulation results where the type of boundary profile was varied. These specified boundary profiles are the experimental mass flux (2.3gm/s), a flat velocity profile (53 m/s) and a parabolic profile (53 m/s centerline velocity). The results are at a location of $z/ID = 4$ and are a grid resolution of $ID/\Delta x = 16$.

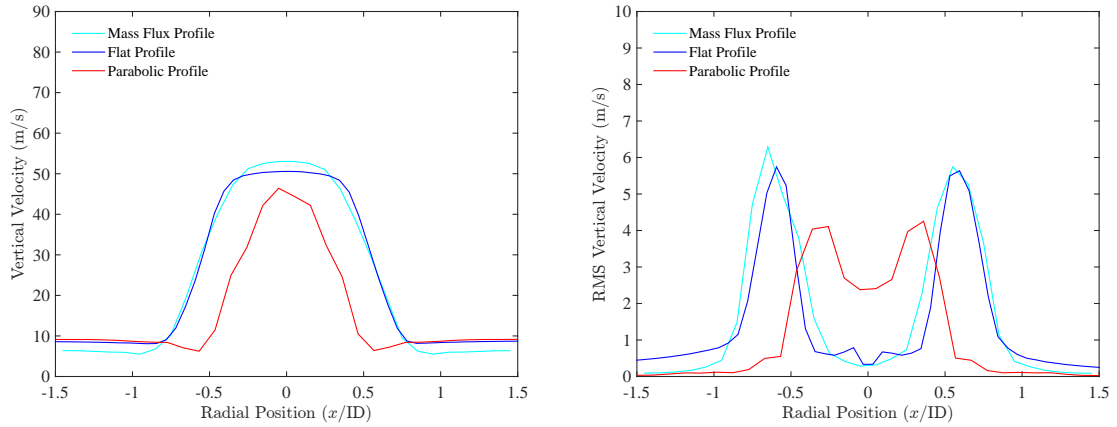


Figure B.10: Jet boundary condition test showing a comparison of the numerical solutions where mass flux, a flat velocity and parabolic velocity conditions were specified. Results show a grid resolution of $ID/\Delta x = 16$. The specified boundary conditions are for the experimental mass flux and centerline velocities of 53 m/s.

Fig. B.11 - B.13 show a set of simulation results where the turbulence model is explored. The simulations use the experimental profile at $z/ID = 4$ where the centerline velocity is set to 69 m/s and the turbulent velocity at the boundary is modified from 10 to 5 to 3 m/s. An increase in turbulent forcing at the boundary results in higher peak fluctuations and lower mean centerline velocities. Fig. B.14 compares these simulation results of the effects of turbulent forcing at the boundary.

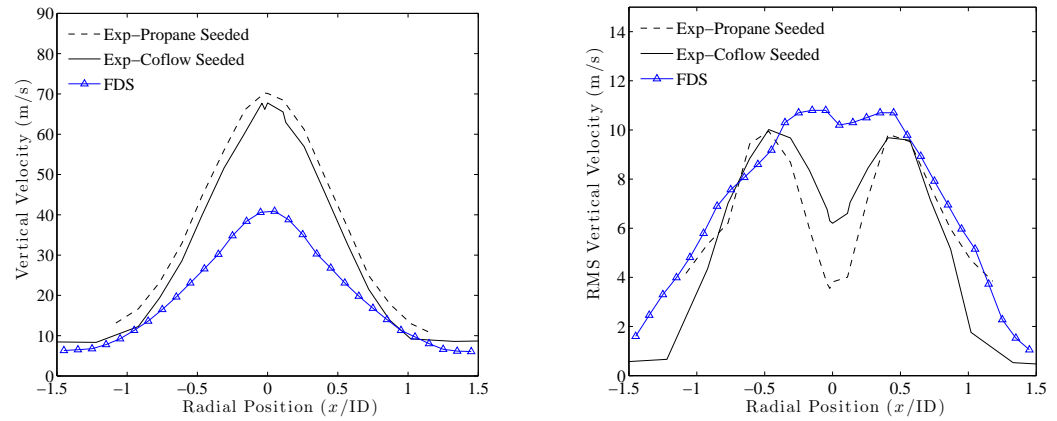


Figure B.11: Jet boundary condition test using the experimental profile at $z/ID = 4$ where the centerline value is set to 69 m/s with a turbulent forcing of 10 m/s at the boundaries. Results show a grid resolution of $ID/\Delta x = 10$.

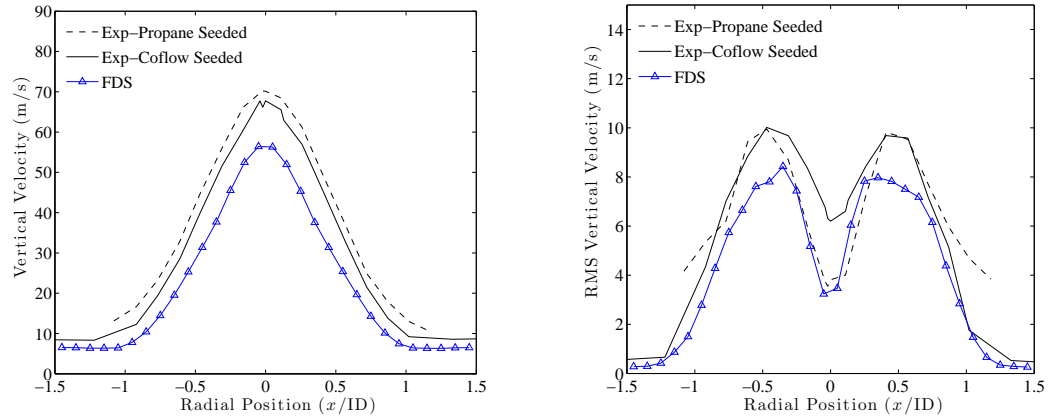


Figure B.12: Jet boundary condition test using the experimental profile at $z/ID = 4$ where the centerline value is set to 69 m/s with a turbulence forcing of 5 m/s at the boundaries. Results show a grid resolution of $ID/\Delta x = 10$.

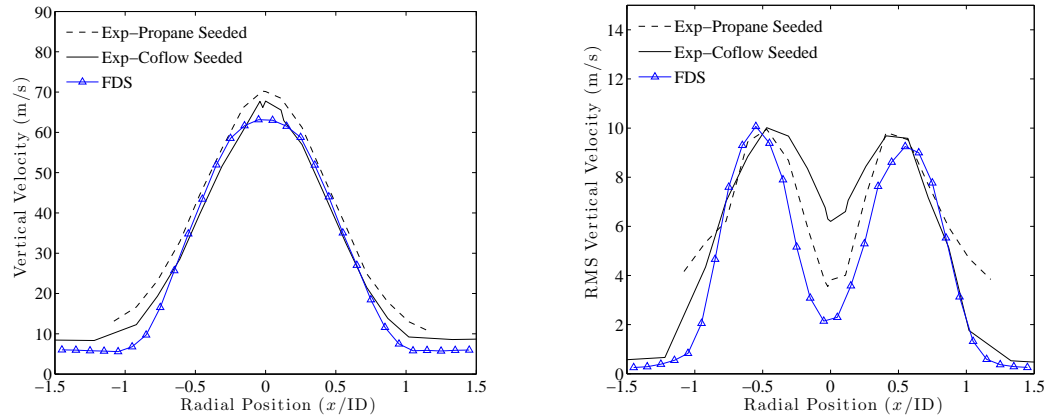


Figure B.13: Jet boundary condition test using the experimental profile at $z/ID = 4$ where the centerline value is set to 69 m/s with a turbulence forcing of 3 m/s at the boundaries. Results show a grid resolution of $ID/\Delta x = 10$.

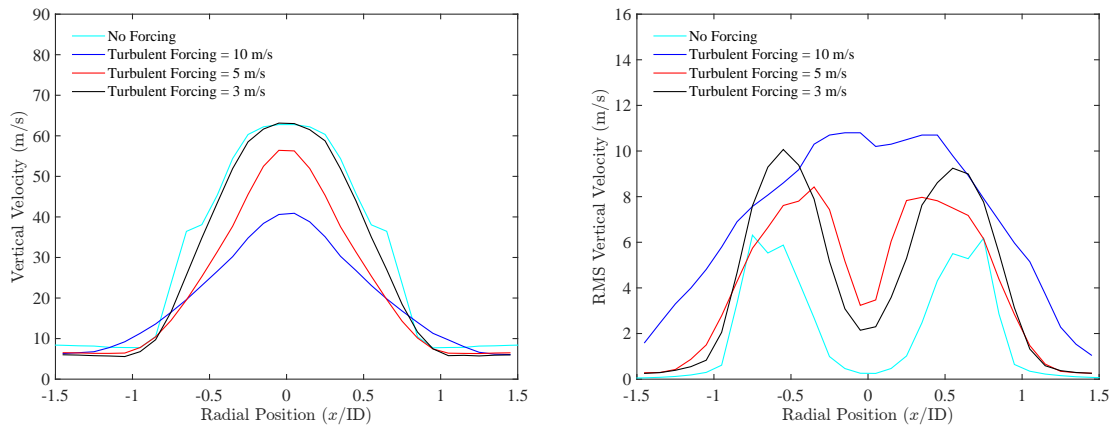


Figure B.14: Simulation test results showing the effect of turbulent forcing at the jet boundary. In these cases, the experimental profile at $z/ID = 4$ is used, where the centerline value is set to 69 m/s. Results show a grid resolution of $ID/\Delta x = 10$.

To better match the peak centerline velocity from the above simulation results, a centerline velocity of 85 m/s is tested. Fig. B.15 show this result with a turbulent forcing of 5 m/s. The asymmetry in the velocity fluctuations is due to the simulation run time being too short. Fig. B.16 shows results with the same jet inlet boundary conditions and uses the Dynamic Smagorinsky turbulence model. As noted, the simulation length is not long enough to accumulate second order statistics. The calculation using the Dynamic Smagorinsky turbulence model takes 28% longer with no effect of the mean vertical velocity profile shape or magnitude. Fig. B.17 shows a baseline simulation with a flat velocity inlet profile with a specified velocity of 85 m/s, no turbulent forcing at the boundary and the default turbulence model.

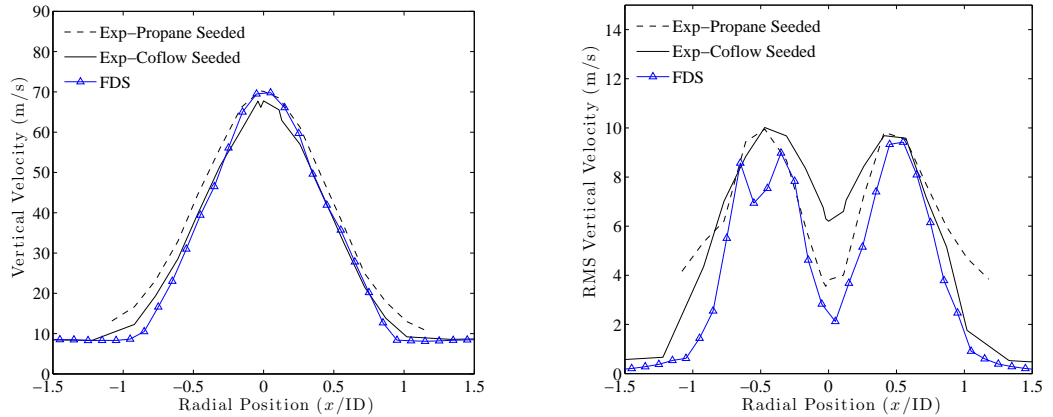


Figure B.15: Jet boundary condition test using the experimental profile at $z/ID = 4$ where the centerline value is set to 85 m/s with a turbulence forcing of 5 m/s at the boundaries. Results show a grid resolution of $ID/\Delta x = 10$.

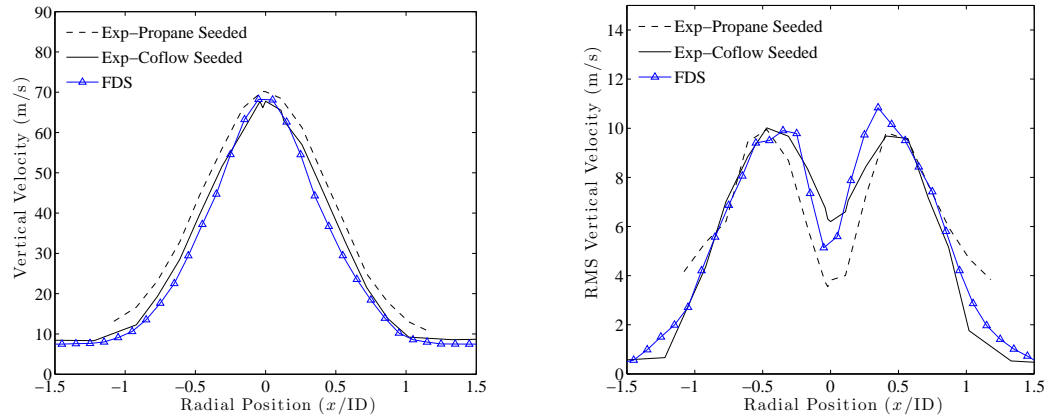


Figure B.16: Jet boundary condition test using the experimental profile at $z/ID = 4$ where the centerline value is set to 85 m/s with a turbulence forcing of 5 m/s at the boundaries. The Dynamic Smagorinsky turbulence model is used. Results show a grid resolution of $ID/\Delta x = 10$.

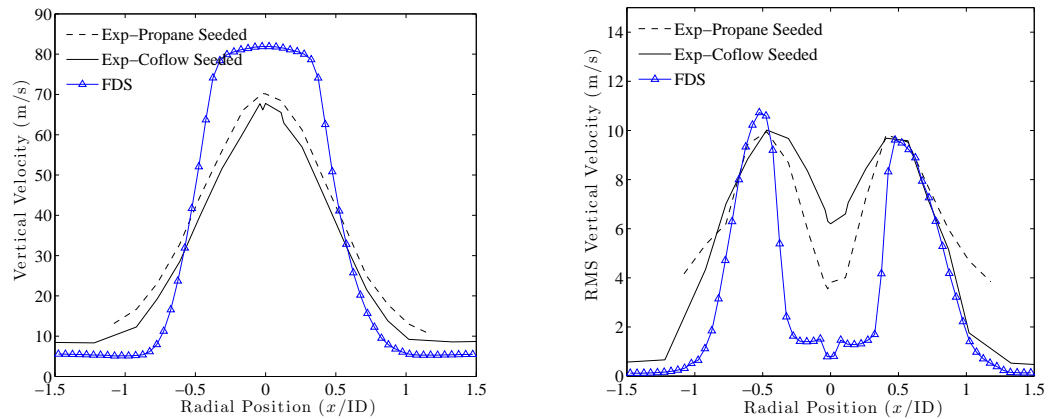


Figure B.17: Jet boundary condition test using a flat profile with a specified velocity of 85 m/s. Results show a grid resolution of $ID/\Delta x = 10$.

Fig. B.18 is shows the results of the effect of the grid resolution where the inlet conditions are specified as a parabolic profile where the centerline velocity is specified as $2u_{bulk}$. At low resolution, FDS under predicted the centerline and peak rms velocities and at higher resolution, the centerline velocity is over predicted and the fluctuations are under predicted.

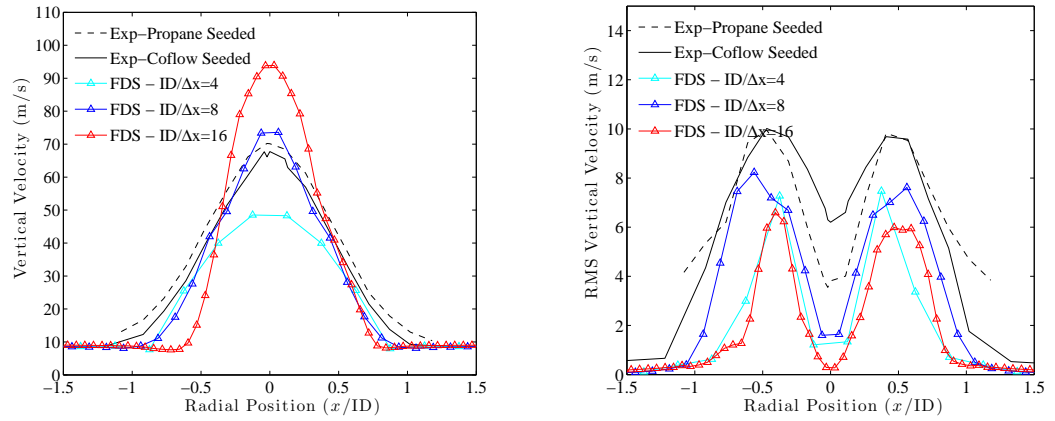


Figure B.18: Jet boundary condition test using a parabolic profile where the centerline velocity is specified as $2u_{bulk}$. Results show grid resolution of $ID/\Delta x = 4, 8$ and 16.

Appendix C: FDS Input Files

C.1 Course Resolution FDS Input File

```
&HEAD CHID='Propane_NonReac_Dodx_8' TITLE='Propane_NonReac_Dodx_8'/

&MULT I D='mesh array 1', DX=0.0208,DY=0.0208,DZ=0.0208,
I_UPPER=1,J_UPPER=1,K_UPPER=8/

&MESH IJK=32,32,32, XB=-0.0208,0,-0.0208,0,0,0.0208,
MULT_ID='mesh array 1' /

&TIME T_END=0.1/

&DUMP DT_DEVC=0.402E-5,
DT_DEVC_LINE=0.09/

&MISC TMPA=21,
SECOND_ORDER_INTERPOLATED_BOUNDARY=.TRUE.,
CONSTANT_SPECIFIC_HEAT_RATIO=.TRUE.,
STRATIFICATION=.FALSE.,
SUPPRESSION=.FALSE.,
W0=9.2,
NEW_OPEN_BOUNDARY=.TRUE./

&RADI RADIATION=.FALSE./

&SPEC ID='PROPANE'/
```

```

&SURF ID='JET',
VEL=-69,
VEL_BULK=-53,
PROFILE='BOUNDARY LAYER',
TAU_MF=0,
TAU_V=0,
MASS_FRACTION(1)=1,
SPEC_ID(1)='PROPANE',
NO_SLIP=.TRUE.,
TMP_FRONT=21/

&SURF ID='TUBE',
DEFAULT=.TRUE.,
TMP_FRONT=21/

&SURF ID='COFLOW',
VEL=-9.2,
TAU_V=0,
TAU_MF=0,
TMP_FRONT=21/

&VENT XB= -0.0026, 0.0026, -0.0026, 0.0026, 0, 0, XYZ=0,0,0,
RADIUS=0.0026, SPREAD_RATE=1E10, SURF_ID='JET', COLOR='RED'/

&VENT XB= -0.0045, 0.0045, -0.0045, 0.0045, 0, 0, XYZ=0,0,0,
RADIUS=0.0045, SURF_ID='TUBE', COLOR='GRAY'/

&VENT XB= -0.0208, 0.0208, -0.0208, 0.0208, 0,0,
SURF_ID='COFLOW', COLOR='POWDER BLUE'/

&VENT PBZ=0.1872,SURF_ID='OPEN'/
&VENT PBY=-0.0208,SURF_ID='OPEN'/
&VENT PBY=0.0208,SURF_ID='OPEN'/
&VENT PBX=-0.0208,SURF_ID='OPEN'/

```

```

&VENT PBX=0.0208,SURF_ID='OPEN'/

&SLCF PBY=0.0013, QUANTITY='VELOCITY', VECTOR=.TRUE./
&SLCF PBY=0.0013, QUANTITY='PRESSURE', CELL_CENTERED=.TRUE./
&SLCF PBY=0.0013, QUANTITY='VISCOSITY', CELL_CENTERED=.TRUE./
&SLCF PBY=0.0013, QUANTITY='DENSITY', CELL_CENTERED=.TRUE./
&SLCF PBY=0.0013, QUANTITY='TEMPERATURE', CELL_CENTERED=.TRUE./
&SLCF PBY=0.0013, QUANTITY='MASS FRACTION', SPEC_ID='PROPANE', CELL_CENTERED=.TRUE./

&BNDF QUANTITY='VELOCITY ERROR'/

&DEVC XYZ=0.001299,0.001299, 0.02079,
QUANTITY='W-VELOCITY', ID='W4' /
&DEVC XYZ=0.001299,0.001299, 0.02079,
QUANTITY='W-VELOCITY', STATISTICS = 'RMS', ID='Wrms4', HIDE_COORDINATES=.TRUE. /

&DEVC XYZ=0.001299,0.001299, 0.0779,
QUANTITY='W-VELOCITY', ID='W15' /
&DEVC XYZ=0.001299,0.001299, 0.0779,
QUANTITY='W-VELOCITY', STATISTICS = 'RMS', ID='Wrms15', HIDE_COORDINATES=.TRUE. /

&DEVC XYZ=0.001299,0.001299, 0.155999,
QUANTITY='W-VELOCITY', ID='W30' /
&DEVC XYZ=0.001299,0.001299, 0.155999,
QUANTITY='W-VELOCITY', STATISTICS = 'RMS', ID='Wrms30', HIDE_COORDINATES=.TRUE. /

&DEVC XYZ=0.001299,0.001299, 0.259999,
QUANTITY='W-VELOCITY', ID='W50' /
&DEVC XYZ=0.001299,0.001299, 0.259999,
QUANTITY='W-VELOCITY', STATISTICS = 'RMS', ID='Wrms50', HIDE_COORDINATES=.TRUE. /

&DEVC XB=-0.020475,0.020475,0.0,0.0,0.02079,0.02079,
QUANTITY='W-VELOCITY', ID='Wmean4', POINTS=64, COORD_FACTOR=192.301/
&DEVC XB=-0.020475,0.020475,0.0,0.0,0.02079,0.02079,

```

QUANTITY='W-VELOCITY', STATISTICS = 'RMS', ID='Wrms4', POINTS=64, HIDE_COORDINATES=.TRUE./
 &DEVC XB=-0.020475,0.020475,0.0,0.0,0.02079,0.02079,
 QUANTITY='CELL U', ID='Umean4', POINTS=64, HIDE_COORDINATES=.TRUE./
 &DEVC XB=-0.020475,0.020475,0.0,0.0,0.02079,0.02079,
 QUANTITY='CELL U', STATISTICS = 'RMS', ID='Urms4', POINTS=64, HIDE_COORDINATES=.TRUE./
 &DEVC XB=-0.020475,0.020475,0.0,0.0,0.02079,0.02079,
 QUANTITY='MASS FRACTION', SPEC_ID='PROPANE', ID='Fmean4', POINTS=64, HIDE_COORDINATES=.TRUE./
 &DEVC XB=-0.020475,0.020475,0.0,0.0,0.02079,0.02079,
 QUANTITY='MASS FRACTION', SPEC_ID='PROPANE', STATISTICS = 'RMS', ID='Frms4', POINTS=64, HIDE_COORDINATES=.TRUE./
 &DEVC XB=-0.020475,0.020475,0.0,0.0,0.02079,0.02079,
 QUANTITY='VISCOSITY', ID='VIS4', POINTS=64, HIDE_COORDINATES=.TRUE./
 &DEVC XB=-0.020475,0.020475,0.0,0.0,0.02079,0.02079,
 QUANTITY='SUBGRID KINETIC ENERGY', ID='KE4', POINTS=64, HIDE_COORDINATES=.TRUE./
 &DEVC XB=-0.020475,0.020475,0.0,0.0,0.02079,0.02079,
 QUANTITY='DENSITY', ID='RH04', POINTS=64, HIDE_COORDINATES=.TRUE./

 &DEVC XB=-0.020475,0.020475,0.0,0.0,0.0779,0.0779,
 QUANTITY='W-VELOCITY', ID='Wmean15', POINTS=64, HIDE_COORDINATES=.TRUE./,
 &DEVC XB=-0.020475,0.020475,0.0,0.0,0.0779,0.0779,
 QUANTITY='W-VELOCITY', STATISTICS = 'RMS', ID='Wrms15', POINTS=64, HIDE_COORDINATES=.TRUE./
 &DEVC XB=-0.020475,0.020475,0.0,0.0,0.0779,0.0779,
 QUANTITY='CELL U', ID='Umean15', POINTS=64, HIDE_COORDINATES=.TRUE./
 &DEVC XB=-0.020475,0.020475,0.0,0.0,0.0779,0.0779,
 QUANTITY='CELL U', STATISTICS = 'RMS', ID='Urms15', POINTS=64, HIDE_COORDINATES=.TRUE./
 &DEVC XB=-0.020475,0.020475,0.0,0.0,0.0779,0.0779,
 QUANTITY='MASS FRACTION', SPEC_ID='PROPANE', ID='Fmean15', POINTS=64, HIDE_COORDINATES=.TRUE./
 &DEVC XB=-0.020475,0.020475,0.0,0.0,0.0779,0.0779,
 QUANTITY='MASS FRACTION', STATISTICS = 'RMS', SPEC_ID='PROPANE', ID='Frms15', POINTS=64, HIDE_COORDINATES=.TRUE./
 &DEVC XB=-0.020475,0.020475,0.0,0.0,0.0779,0.0779,
 QUANTITY='VISCOSITY', ID='VIS15', POINTS=64, HIDE_COORDINATES=.TRUE./
 &DEVC XB=-0.020475,0.020475,0.0,0.0,0.0779,0.0779,
 QUANTITY='SUBGRID KINETIC ENERGY', ID='KE15', POINTS=64, HIDE_COORDINATES=.TRUE./
 &DEVC XB=-0.020475,0.020475,0.0,0.0,0.0779,0.0779,
 QUANTITY='DENSITY', ID='RH015', POINTS=64, HIDE_COORDINATES=.TRUE./

```

&DEVC XB=-0.020475,0.020475,0.0,0.0,0.155999,0.155999,
QUANTITY='W-VELOCITY', ID='Wmean30', POINTS=64, HIDE_COORDINATES=.TRUE./
&DEVC XB=-0.020475,0.020475,0.0,0.0,0.155999,0.155999,
QUANTITY='W-VELOCITY', STATISTICS = 'RMS', ID='Wrms30', POINTS=64, HIDE_COORDINATES=.TRUE./
&DEVC XB=-0.020475,0.020475,0.0,0.0,0.155999,0.155999,
QUANTITY='CELL U', ID='Umean30', POINTS=64, HIDE_COORDINATES=.TRUE./
&DEVC XB=-0.020475,0.020475,0.0,0.0,0.155999,0.155999,
QUANTITY='CELL U', STATISTICS = 'RMS', ID='Urms30', POINTS=64, HIDE_COORDINATES=.TRUE./
&DEVC XB=-0.020475,0.020475,0.0,0.0,0.155999,0.155999,
QUANTITY='MASS FRACTION', SPEC_ID='PROPANE', ID='Fmean30', POINTS=64, HIDE_COORDINATES=.TRUE./
&DEVC XB=-0.020475,0.020475,0.0,0.0,0.155999,0.155999,
QUANTITY='MASS FRACTION', STATISTICS = 'RMS', SPEC_ID='PROPANE', ID='Frms30', POINTS=64, HIDE_COORDINATES=.TRUE./
&DEVC XB=-0.020475,0.020475,0.0,0.0,0.155999,0.155999,
QUANTITY='VISCOSITY', ID='VIS30', POINTS=64, HIDE_COORDINATES=.TRUE./
&DEVC XB=-0.020475,0.020475,0.0,0.0,0.155999,0.155999,
QUANTITY='SUBGRID KINETIC ENERGY', ID='KE30', POINTS=64, HIDE_COORDINATES=.TRUE./
&DEVC XB=-0.020475,0.020475,0.0,0.0,0.155999,0.155999,
QUANTITY='DENSITY', ID='RH030', POINTS=64, HIDE_COORDINATES=.TRUE./

&DEVC XB=-0.02015,0.02015,0.0,0.0,0.259999,0.259999,
QUANTITY='W-VELOCITY', ID='Wmean50', POINTS=32, COORD_FACTOR=192.301/
&DEVC XB=-0.02015,0.02015,0.0,0.0,0.259999,0.259999,
QUANTITY='W-VELOCITY', STATISTICS = 'RMS', ID='Wrms50', POINTS=32, HIDE_COORDINATES=.TRUE./
&DEVC XB=-0.02015,0.02015,0.0,0.0,0.259999,0.259999,
QUANTITY='CELL U', ID='Umean50', POINTS=32, HIDE_COORDINATES=.TRUE./
&DEVC XB=-0.02015,0.02015,0.0,0.0,0.259999,0.259999,
QUANTITY='CELL U', STATISTICS = 'RMS', ID='Urms50', POINTS=32, HIDE_COORDINATES=.TRUE./
&DEVC XB=-0.02015,0.02015,0.0,0.0,0.259999,0.259999,
QUANTITY='MASS FRACTION', SPEC_ID='PROPANE', ID='Fmean50', POINTS=32, HIDE_COORDINATES=.TRUE./
&DEVC XB=-0.02015,0.02015,0.0,0.0,0.259999,0.259999,
QUANTITY='MASS FRACTION', STATISTICS = 'RMS', SPEC_ID='PROPANE', ID='Frms50', POINTS=32, HIDE_COORDINATES=.TRUE./
&DEVC XB=-0.02015,0.02015,0.0,0.0,0.259999,0.259999,
QUANTITY='VISCOSITY', ID='VIS50', POINTS=32, HIDE_COORDINATES=.TRUE./

```

```

&DEVC XB=-0.02015,0.02015,0.0,0.0,0.259999,0.259999,
QUANTITY='SUBGRID KINETIC ENERGY', ID='KE50', POINTS=32, HIDE_COORDINATES=.TRUE./
&DEVC XB=-0.02015,0.02015,0.0,0.0,0.259999,0.259999,
QUANTITY='DENSITY', ID='RH050', POINTS=64, HIDE_COORDINATES=.TRUE./

&DEVC XB=0,0,0.0,0.0,0.00065,0.26975,
QUANTITY='W-VELOCITY', ID='CL Wmean', COORD_FACTOR=192.301, POINTS=208/
&DEVC XB=0,0,0.0,0.0,0.00065,0.26975,
QUANTITY='W-VELOCITY', ID='CL Wrms', STATISTICS = 'RMS', POINTS=208, HIDE_COORDINATES=.TRUE. /
&DEVC XB=0,0,0.0,0.0,0.00065,0.26975,
QUANTITY='U-VELOCITY', ID='CL Umean', POINTS=208, HIDE_COORDINATES=.TRUE. /
&DEVC XB=0,0,0.0,0.0,0.00065,0.26975,
QUANTITY='U-VELOCITY', ID='CL Urms', STATISTICS = 'RMS', POINTS=208, HIDE_COORDINATES=.TRUE. /
&DEVC XB=0,0,0.0,0.0,0.00065,0.26975,
QUANTITY='MASS FRACTION', SPEC_ID='PROPANE', ID='CL Fmean', POINTS=208, HIDE_COORDINATES=.TRUE. /
&DEVC XB=0,0,0.0,0.0,0.00065,0.26975,
QUANTITY='MASS FRACTION', SPEC_ID='PROPANE', STATISTICS = 'RMS', ID='CL Frms', POINTS=208, HIDE_COORDINATES=.TRUE. /
&DEVC XB=0,0,0.0,0.0,0.00065,0.26975,
QUANTITY='SUBGRID KINETIC ENERGY', ID='CL KE', POINTS=208, HIDE_COORDINATES=.TRUE. /
&DEVC XB=0,0,0.0,0.0,0.00065,0.26975,
QUANTITY='DENSITY', ID='CL RHO', POINTS=208, HIDE_COORDINATES=.TRUE. /
&DEVC XB=0,0,0.0,0.0,0.00065,0.26975,
QUANTITY='VISCOSITY', ID='CL VIS', POINTS=208, HIDE_COORDINATES=.TRUE. /

&DEVC XB=-0.002275,0.002275,0,0,0.0000001,0.0000001,
QUANTITY='NORMAL VELOCITY', IOR=3, ID='Wmean BC', POINTS=8, COORD_FACTOR=192.301/
&DEVC XB=-0.002275,0.002275,0,0,0.0000001,0.0000001,
QUANTITY='DENSITY', ID='RHO BC', POINTS=8, HIDE_COORDINATES=.TRUE./
&DEVC XB=-0.002275,0.002275,0,0,0.0000001,0.0000001,
QUANTITY='MASS FRACTION', SPEC_ID='PROPANE', ID='MASS FRACTION BC', POINTS=8, HIDE_COORDINATES=.TRUE./

&TAIL/

```

C.2 Medium Resolution FDS Input File

```
&HEAD CHID='Propane_NonReac_Dodx_16' TITLE='Propane_NonReac_Dodx_16'/

&MULT ID='mesh array 1', DX=0.0104,DY=0.0104,DZ=0.0104,
I_UPPER=1,J_UPPER=1,K_UPPER=3/
&MESH IJK=32,32,32, XB=-0.0104,0,-0.0104,0,0,0.0104,
MULT_ID='mesh array 1' /

&MULT ID='mesh array 2', DX=0,DY=0,DZ=0.0208,
I_UPPER=0,J_UPPER=0,K_UPPER=1/
&MESH IJK= 16,48,32, XB=0.0104,0.0208,0.0104,-0.0208,0.0,0.0208,
MULT_ID='mesh array 2' /
&MESH IJK= 48,16,32, XB=-0.0104,0.0208,0.0104,0.0208,0.0,0.0208,
MULT_ID='mesh array 2' /
&MESH IJK= 16,48,32, XB=-0.0104,-0.0208,-0.0104,0.0208,0.0,0.0208,
MULT_ID='mesh array 2' /
&MESH IJK= 48,16,32, XB=0.0104,-0.0208,-0.0104,-0.0208,0.0,0.0208,
MULT_ID='mesh array 2' /

&MULT ID='mesh array 3', DX=0.0208,DY=0.0208,DZ=0.0208,
I_UPPER=1,J_UPPER=1,K_UPPER=3/
&MESH IJK=32,32,32, XB=-0.0208,0,-0.0208,0,0.0416,0.0624,
MULT_ID='mesh array 3' /

&MULT ID='mesh array 4', DX=0,DY=0,DZ=0.0416,
I_UPPER=0,J_UPPER=0,K_UPPER=1/
&MESH IJK=32,32,32, XB=-0.0208,0.0208,-0.0208,0.0208,0.1248,0.1664,
MULT_ID='mesh array 4' /

&TIME T_END=0.1/

&DUMP DT_DEVC=0.201E-5,
```

DT_DEVC_LINE=0.09/

&MISC TMPA=21,
SECOND_ORDER_INTERPOLATED_BOUNDARY=.TRUE. ,
CONSTANT_SPECIFIC_HEAT_RATIO=.TRUE. ,
STRATIFICATION=.FALSE. ,
SUPPRESSION=.FALSE. ,
WO=9.2,
NEW_OPEN_BOUNDARY=.TRUE. /

&RADI RADIATION=.FALSE. /

&SPEC ID='PROPANE' /

&SURF ID='JET' ,
VEL=-69 ,
VEL_BULK=-53 ,
PROFILE='BOUNDARY LAYER' ,
TAU_MF=0 ,
TAU_V=0 ,
MASS_FRACTION(1)=1 ,
SPEC_ID(1)='PROPANE' ,
TMP_FRONT=21 ,
NO_SLIP=.TRUE. /

&SURF ID='TUBE' ,
DEFAULT=.TRUE. ,
TMP_FRONT=21 /

&SURF ID='COFLOW' ,
VEL=-9.2 ,
TAU_V=0 ,
TAU_MF=0 ,
TMP_FRONT=21 /

```

&VENT XB= -0.0026, 0.0026, -0.0026, 0.0026, 0, 0, XYZ=0,0,0,
RADIUS=0.0026, SPREAD_RATE=1E10, SURF_ID='JET', COLOR='RED'/

&VENT XB= -0.0045, 0.0045, -0.0045, 0.0045, 0, 0, XYZ=0,0,0,
RADIUS=0.0045, SURF_ID='TUBE', COLOR='GRAY'/

&VENT XB= -0.0208, 0.0208, -0.0208, 0.0208, 0,0,
SURF_ID='COFLOW', COLOR='POWDER BLUE'/

&VENT PBZ=0.208,SURF_ID='OPEN'/
&VENT PBY=-0.0208,SURF_ID='OPEN'/
&VENT PBY=0.0208,SURF_ID='OPEN'/
&VENT PBX=-0.0208,SURF_ID='OPEN'/
&VENT PBX=0.0208,SURF_ID='OPEN'/

&SLCF PBY=0.0013, QUANTITY='VELOCITY', VECTOR=.TRUE./
&SLCF PBY=0.0013, QUANTITY='PRESSURE', CELL_CENTERED=.TRUE./
&SLCF PBY=0.0013, QUANTITY='VISCOSITY', CELL_CENTERED=.TRUE./
&SLCF PBY=0.0013, QUANTITY='DENSITY', CELL_CENTERED=.TRUE./
&SLCF PBY=0.0013, QUANTITY='TEMPERATURE', CELL_CENTERED=.TRUE./
&SLCF PBY=0.0013, QUANTITY='MASS FRACTION', SPEC_ID='PROPANE', CELL_CENTERED=.TRUE./
&SLCF PBY=0.0013, QUANTITY='MACH NUMBER', CELL_CENTERED=.TRUE./

&BNDF QUANTITY='VELOCITY ERROR'/

&DEVC XYZ=0.001299,0.001299, 0.02079,
QUANTITY='W-VELOCITY', ID='W4' /
&DEVC XYZ=0.001299,0.001299, 0.02079,
QUANTITY='W-VELOCITY', STATISTICS = 'RMS', ID='Wrms4', HIDE_COORDINATES=.TRUE. /

&DEVC XYZ=0.001299,0.001299, 0.0779,
QUANTITY='W-VELOCITY', ID='W15' /
&DEVC XYZ=0.001299,0.001299, 0.0779,

```

```

QUANTITY='W-VELOCITY', STATISTICS = 'RMS', ID='Wrms15', HIDE_COORDINATES=.TRUE. /

&DEVC XYZ=0.001299,0.001299, 0.155999,

QUANTITY='W-VELOCITY', ID='W30' /

&DEVC XYZ=0.001299,0.001299, 0.155999,

QUANTITY='W-VELOCITY', STATISTICS = 'RMS', ID='Wrms30', HIDE_COORDINATES=.TRUE. /

DEVC XYZ=0.001299,0.001299, 0.259999,

QUANTITY='W-VELOCITY', ID='W50' /

DEVC XYZ=0.001299,0.001299, 0.259999,

QUANTITY='W-VELOCITY', STATISTICS = 'RMS', ID='Wrms50', HIDE_COORDINATES=.TRUE. /

&DEVC XB=-0.020475,0.020475,0.0,0.0,0.02079,0.02079,

QUANTITY='W-VELOCITY', ID='Wmean4', POINTS=64, COORD_FACTOR=192.301/

&DEVC XB=-0.020475,0.020475,0.0,0.0,0.02079,0.02079,

QUANTITY='W-VELOCITY', STATISTICS = 'RMS', ID='Wrms4', POINTS=64, HIDE_COORDINATES=.TRUE./

&DEVC XB=-0.020475,0.020475,0.0,0.0,0.02079,0.02079,

QUANTITY='CELL U', ID='Umean4', POINTS=64, HIDE_COORDINATES=.TRUE./

&DEVC XB=-0.020475,0.020475,0.0,0.0,0.02079,0.02079,

QUANTITY='CELL U', STATISTICS = 'RMS', ID='Urms4', POINTS=64, HIDE_COORDINATES=.TRUE./

&DEVC XB=-0.020475,0.020475,0.0,0.0,0.02079,0.02079,

QUANTITY='MASS FRACTION', SPEC_ID='PROPANE', ID='Fmean4', POINTS=64, HIDE_COORDINATES=.TRUE./

&DEVC XB=-0.020475,0.020475,0.0,0.0,0.02079,0.02079,

QUANTITY='MASS FRACTION', STATISTICS = 'RMS', SPEC_ID='PROPANE', ID='Frms4', POINTS=64, HIDE_COORDINATES=.TRUE./

&DEVC XB=-0.020475,0.020475,0.0,0.0,0.02079,0.02079,

QUANTITY='VISCOSITY', ID='VIS4', POINTS=64, HIDE_COORDINATES=.TRUE./

&DEVC XB=-0.020475,0.020475,0.0,0.0,0.02079,0.02079,

QUANTITY='SUBGRID KINETIC ENERGY', ID='KE4', POINTS=64, HIDE_COORDINATES=.TRUE./

&DEVC XB=-0.020475,0.020475,0.0,0.0,0.02079,0.02079,

QUANTITY='DENSITY', ID='RH04', POINTS=64, HIDE_COORDINATES=.TRUE./

&DEVC XB=-0.020475,0.020475,0.0,0.0,0.0779,0.0779,

QUANTITY='W-VELOCITY', ID='Wmean15', POINTS=64, HIDE_COORDINATES=.TRUE./

&DEVC XB=-0.020475,0.020475,0.0,0.0,0.0779,0.0779,

```

QUANTITY='W-VELOCITY', STATISTICS = 'RMS', ID='Wrms15', POINTS=64, HIDE_COORDINATES=.TRUE./
 &DEVC XB=-0.020475,0.020475,0.0,0.0,0.0779,0.0779,
 QUANTITY='CELL U', ID='Umean15', POINTS=64, HIDE_COORDINATES=.TRUE./
 &DEVC XB=-0.020475,0.020475,0.0,0.0,0.0779,0.0779,
 QUANTITY='CELL U', STATISTICS = 'RMS', ID='Urms15', POINTS=64, HIDE_COORDINATES=.TRUE./
 &DEVC XB=-0.020475,0.020475,0.0,0.0,0.0779,0.0779,
 QUANTITY='MASS FRACTION', SPEC_ID='PROPANE', ID='Fmean15', POINTS=64, HIDE_COORDINATES=.TRUE./
 &DEVC XB=-0.020475,0.020475,0.0,0.0,0.0779,0.0779,
 QUANTITY='MASS FRACTION', STATISTICS = 'RMS', SPEC_ID='PROPANE', ID='Frms15', POINTS=64, HIDE_COORDINATES=.TRUE./
 &DEVC XB=-0.020475,0.020475,0.0,0.0,0.0779,0.0779,
 QUANTITY='VISCOSITY', ID='VIS15', POINTS=64, HIDE_COORDINATES=.TRUE./
 &DEVC XB=-0.020475,0.020475,0.0,0.0,0.0779,0.0779,
 QUANTITY='SUBGRID KINETIC ENERGY', ID='KE15', POINTS=64, HIDE_COORDINATES=.TRUE./
 &DEVC XB=-0.020475,0.020475,0.0,0.0,0.0779,0.0779,
 QUANTITY='DENSITY', ID='RHO15', POINTS=64, HIDE_COORDINATES=.TRUE./

 &DEVC XB=-0.02015,0.02015,0.0,0.0,0.155999,0.155999,
 QUANTITY='W-VELOCITY', ID='Wmean30', POINTS=32, COORD_FACTOR=192.301/
 &DEVC XB=-0.02015,0.02015,0.0,0.0,0.155999,0.155999,
 QUANTITY='W-VELOCITY', STATISTICS = 'RMS', ID='Wrms30', POINTS=32, HIDE_COORDINATES=.TRUE./
 &DEVC XB=-0.02015,0.02015,0.0,0.0,0.155999,0.155999,
 QUANTITY='CELL U', ID='Umean30', POINTS=32, HIDE_COORDINATES=.TRUE./
 &DEVC XB=-0.02015,0.02015,0.0,0.0,0.155999,0.155999,
 QUANTITY='CELL U', STATISTICS = 'RMS', ID='Urms30', POINTS=32, HIDE_COORDINATES=.TRUE./
 &DEVC XB=-0.02015,0.02015,0.0,0.0,0.155999,0.155999,
 QUANTITY='MASS FRACTION', SPEC_ID='PROPANE', ID='Fmean30', POINTS=32, HIDE_COORDINATES=.TRUE./
 &DEVC XB=-0.02015,0.02015,0.0,0.0,0.155999,0.155999,
 QUANTITY='MASS FRACTION', STATISTICS = 'RMS', SPEC_ID='PROPANE', ID='Frms30', POINTS=32, HIDE_COORDINATES=.TRUE./
 &DEVC XB=-0.02015,0.02015,0.0,0.0,0.155999,0.155999,
 QUANTITY='VISCOSITY', ID='VIS30', POINTS=32, HIDE_COORDINATES=.TRUE./
 &DEVC XB=-0.02015,0.02015,0.0,0.0,0.155999,0.155999,
 QUANTITY='SUBGRID KINETIC ENERGY', ID='KE30', POINTS=32, HIDE_COORDINATES=.TRUE./
 &DEVC XB=-0.02015,0.02015,0.0,0.0,0.155999,0.155999,
 QUANTITY='DENSITY', ID='RHO30', POINTS=32, HIDE_COORDINATES=.TRUE./

```

&DEVC XB=0,0,0.0,0.0,0.0,0.1664,
QUANTITY='W-VELOCITY', ID='CL Wmean', COORD_FACTOR=192.301, POINTS=129/
&DEVC XB=0,0,0.0,0.0,0.0,0.1664,
QUANTITY='W-VELOCITY', ID='CL Wrms', STATISTICS = 'RMS', POINTS=129, HIDE_COORDINATES=.TRUE. /
&DEVC XB=0,0,0.0,0.0,0.0,0.1664,
QUANTITY='U-VELOCITY', ID='CL Umean', POINTS=129, HIDE_COORDINATES=.TRUE. /
&DEVC XB=0,0,0.0,0.0,0.0,0.1664,
QUANTITY='U-VELOCITY', ID='CL Urms', STATISTICS = 'RMS', POINTS=129, HIDE_COORDINATES=.TRUE. /
&DEVC XB=0,0,0.0,0.0,0.0,0.1664,
QUANTITY='MASS FRACTION', SPEC_ID='PROPANE', ID='CL Fmean', POINTS=129, HIDE_COORDINATES=.TRUE. /

&DEVC XB=0,0,0.0,0.0,0.0,0.1664,
QUANTITY='MASS FRACTION', SPEC_ID='PROPANE', STATISTICS = 'RMS', ID='CL Frms', POINTS=129, HIDE_COORDINATES=.TRUE. /
&DEVC XB=0,0,0.0,0.0,0.0,0.1664,
QUANTITY='SUBGRID KINETIC ENERGY', ID='CL KE', POINTS=129, HIDE_COORDINATES=.TRUE. /
&DEVC XB=0,0,0.0,0.0,0.0,0.1664,
QUANTITY='DENSITY', ID='CL RHO', POINTS=129, HIDE_COORDINATES=.TRUE. /

&DEVC XB=-0.002438,0.002438,0,0,0.0000001,0.0000001,
QUANTITY='NORMAL VELOCITY', IOR=3, ID='Wmean BC', POINTS=16, COORD_FACTOR=192.301/
&DEVC XB=-0.002438,0.002438,0,0,0.0000001,0.0000001,
QUANTITY='DENSITY', ID='RHO BC', POINTS=16, HIDE_COORDINATES=.TRUE./
&DEVC XB=-0.002438,0.002438,0,0,0.0000001,0.0000001,
QUANTITY='MASS FRACTION', SPEC_ID='PROPANE', ID='MASS FRACTION BC', POINTS=16, HIDE_COORDINATES=.TRUE./

&TAIL/

```

C.3 Fine Resolution FDS Input File

```

&HEAD CHID='Propane_NonReac_Dodx_32' TITLE='Propane_NonReac_Dodx_32'/

```

```

&MULT ID='mesh array 1', DX=0.0104,DY=0.0104,DZ=0.0104,
I_UPPER=1,J_UPPER=1,K_UPPER=3/
&MESH IJK=64,64,64, XB=-0.0104,0,-0.0104,0,0,0.0104, MULT_ID='mesh array 1' /

&MULT ID='mesh array 2', DX=0,DY=0,DZ=0.0208,
I_UPPER=0,J_UPPER=0,K_UPPER=1/
&MESH IJK= 32,96,64, XB=0.0104,0.0208,0.0104,-0.0208,0.0,0.0208, MULT_ID='mesh array 2' /
&MESH IJK= 96,32,64, XB=-0.0104,0.0208,0.0104,0.0208,0.0,0.0208, MULT_ID='mesh array 2' /
&MESH IJK= 32,96,64, XB=-0.0104,-0.0208,-0.0104,0.0208,0.0,0.0208, MULT_ID='mesh array 2' /
&MESH IJK= 96,32,64, XB=0.0104,-0.0208,-0.0104,-0.0208,0.0,0.0208, MULT_ID='mesh array 2' /

&MULT ID='mesh array 3', DX=0.0208,DY=0.0208,DZ=0.0208,
I_UPPER=1,J_UPPER=1,K_UPPER=3/
&MESH IJK=64,64,64, XB=-0.0208,0,-0.0208,0,0.0416,0.0624, MULT_ID='mesh array 3' /

&MULT ID='mesh array 4', DX=0,DY=0,DZ=0.0416,
I_UPPER=0,J_UPPER=0,K_UPPER=1/
&MESH IJK=64,64,64, XB=-0.0208,0.0208,-0.0208,0.0208,0.1248,0.1664, MULT_ID='mesh array 4' /

&TIME T_END=0.1/

&DUMP DT_DEVC=0.101E-5,
DT_DEVC_LINE=0.09/

&MISC TMPA=21,
SECOND_ORDER_INTERPOLATED_BOUNDARY=.TRUE.,
CONSTANT_SPECIFIC_HEAT_RATIO=.TRUE.,
STRATIFICATION=.FALSE.,
SUPPRESSION=.FALSE.,
W0=9.2,
NEW_OPEN_BOUNDARY=.TRUE./

&RADI RADIATION=.FALSE./

```

&SPEC ID='PROPANE' /

&SURF ID='JET',

VEL=-69,

VEL_BULK=-53,

PROFILE='BOUNDARY LAYER',

TAU_MF=0,

TAU_V=0,

MASS_FRACTION(1)=1,

SPEC_ID(1)='PROPANE',

TMP_FRONT=21,

NO_SLIP=.TRUE. /

&SURF ID='TUBE',

DEFAULT=.TRUE. ,

TMP_FRONT=21/

&SURF ID='COFLOW',

VEL=-9.2,

TAU_V=0,

TAU_MF=0,

TMP_FRONT=21/

&VENT XB= -0.0026, 0.0026, -0.0026, 0.0026, 0, 0, XYZ=0,0,0,

RADIUS=0.0026, SPREAD_RATE=1E10, SURF_ID='JET', COLOR='RED' /

&VENT XB= -0.0045, 0.0045, -0.0045, 0.0045, 0, 0, XYZ=0,0,0,

RADIUS=0.0045, SURF_ID='TUBE', COLOR='GRAY' /

&VENT XB= -0.0208, 0.0208, -0.0208, 0.0208, 0,0,

SURF_ID='COFLOW', COLOR='POWDER BLUE' /

&VENT PBZ=0.208, SURF_ID='OPEN' /

```

&VENT  PBX=-0.0208,SURF_ID='OPEN'/
&VENT  PBY=0.0208,SURF_ID='OPEN'/
&VENT  PBX=-0.0208,SURF_ID='OPEN'/
&VENT  PBX=0.0208,SURF_ID='OPEN'/

&SLCF  PBY=0.0013, QUANTITY='VELOCITY', VECTOR=.TRUE./
&SLCF  PBY=0.0013, QUANTITY='PRESSURE', CELL_CENTERED=.TRUE./
&SLCF  PBY=0.0013, QUANTITY='VISCOSITY', CELL_CENTERED=.TRUE./
&SLCF  PBY=0.0013, QUANTITY='DENSITY', CELL_CENTERED=.TRUE./
&SLCF  PBY=0.0013, QUANTITY='TEMPERATURE', CELL_CENTERED=.TRUE./
&SLCF  PBY=0.0013, QUANTITY='MASS FRACTION', SPEC_ID='PROPANE', CELL_CENTERED=.TRUE./
&SLCF  PBY=0.0013, QUANTITY='MACH NUMBER', CELL_CENTERED=.TRUE./

&BNDF  QUANTITY='VELOCITY ERROR'/

&DEVC  XYZ=0.001299,0.001299, 0.02079,
QUANTITY='W-VELOCITY', ID='W4' /
&DEVC  XYZ=0.001299,0.001299, 0.02079,
QUANTITY='W-VELOCITY', STATISTICS = 'RMS', ID='Wrms4', HIDE_COORDINATES=.TRUE. /

&DEVC  XYZ=0.001299,0.001299, 0.0779,
QUANTITY='W-VELOCITY', ID='W15' /
&DEVC  XYZ=0.001299,0.001299, 0.0779,
QUANTITY='W-VELOCITY', STATISTICS = 'RMS', ID='Wrms15', HIDE_COORDINATES=.TRUE. /

&DEVC  XYZ=0.001299,0.001299, 0.155999,
QUANTITY='W-VELOCITY', ID='W30' /
&DEVC  XYZ=0.001299,0.001299, 0.155999,
QUANTITY='W-VELOCITY', STATISTICS = 'RMS', ID='Wrms30', HIDE_COORDINATES=.TRUE. /

DEVC  XYZ=0.001299,0.001299, 0.259999,
QUANTITY='W-VELOCITY', ID='W50' /
DEVC  XYZ=0.001299,0.001299, 0.259999,
QUANTITY='W-VELOCITY', STATISTICS = 'RMS', ID='Wrms50', HIDE_COORDINATES=.TRUE. /

```

```

&DEVC XB=-0.020638,0.020638,0.0,0.0,0.02079,0.02079,
QUANTITY='W-VELOCITY', ID='Wmean4', POINTS=128, COORD_FACTOR=192.301/
&DEVC XB=-0.020638,0.020638,0.0,0.0,0.02079,0.02079,
QUANTITY='W-VELOCITY', STATISTICS = 'RMS', ID='Wrms4', POINTS=128, HIDE_COORDINATES=.TRUE./
&DEVC XB=-0.020638,0.020638,0.0,0.0,0.02079,0.02079,
QUANTITY='CELL U', ID='Umean4', POINTS=128, HIDE_COORDINATES=.TRUE./
&DEVC XB=-0.020638,0.020638,0.0,0.0,0.02079,0.02079,
QUANTITY='CELL U', STATISTICS = 'RMS', ID='Urms4', POINTS=128, HIDE_COORDINATES=.TRUE./
&DEVC XB=-0.020638,0.020638,0.0,0.0,0.02079,0.02079,
QUANTITY='MASS FRACTION', SPEC_ID='PROPANE', ID='Fmean4', POINTS=128, HIDE_COORDINATES=.TRUE./
&DEVC XB=-0.020638,0.020638,0.0,0.0,0.02079,0.02079,
QUANTITY='MASS FRACTION', STATISTICS = 'RMS', SPEC_ID='PROPANE', ID='Frms4', POINTS=128, HIDE_COORDINATES=.TRUE./
&DEVC XB=-0.020638,0.020638,0.0,0.0,0.02079,0.02079,
QUANTITY='VISCOSITY', ID='VIS4', POINTS=128, HIDE_COORDINATES=.TRUE./
&DEVC XB=-0.020638,0.020638,0.0,0.0,0.02079,0.02079,
QUANTITY='SUBGRID KINETIC ENERGY', ID='KE4', POINTS=128, HIDE_COORDINATES=.TRUE./
&DEVC XB=-0.020638,0.020638,0.0,0.0,0.02079,0.02079,
QUANTITY='DENSITY', ID='RHO4', POINTS=128, HIDE_COORDINATES=.TRUE./

&DEVC XB=-0.020638,0.020638,0.0,0.0,0.0779,0.0779,
QUANTITY='W-VELOCITY', ID='Wmean15', POINTS=128, HIDE_COORDINATES=.TRUE./
&DEVC XB=-0.020638,0.020638,0.0,0.0,0.0779,0.0779,
QUANTITY='W-VELOCITY', STATISTICS = 'RMS', ID='Wrms15', POINTS=128, HIDE_COORDINATES=.TRUE./
&DEVC XB=-0.020638,0.020638,0.0,0.0,0.0779,0.0779,
QUANTITY='CELL U', ID='Umean15', POINTS=128, HIDE_COORDINATES=.TRUE./
&DEVC XB=-0.020638,0.020638,0.0,0.0,0.0779,0.0779,
QUANTITY='CELL U', STATISTICS = 'RMS', ID='Urms15', POINTS=128, HIDE_COORDINATES=.TRUE./
&DEVC XB=-0.020638,0.020638,0.0,0.0,0.0779,0.0779,
QUANTITY='MASS FRACTION', SPEC_ID='PROPANE', ID='Fmean15', POINTS=128, HIDE_COORDINATES=.TRUE./
&DEVC XB=-0.020638,0.020638,0.0,0.0,0.0779,0.0779,
QUANTITY='MASS FRACTION', STATISTICS = 'RMS', SPEC_ID='PROPANE', ID='Frms15', POINTS=128, HIDE_COORDINATES=.TRUE./
&DEVC XB=-0.020638,0.020638,0.0,0.0,0.0779,0.0779,
QUANTITY='VISCOSITY', ID='VIS15', POINTS=128, HIDE_COORDINATES=.TRUE./

```

```

&DEVC XB=-0.020638,0.020638,0.0,0.0,0.0779,0.0779,
QUANTITY='SUBGRID KINETIC ENERGY', ID='KE15', POINTS=128, HIDE_COORDINATES=.TRUE./
&DEVC XB=-0.020638,0.020638,0.0,0.0,0.0779,0.0779,
QUANTITY='DENSITY', ID='RH015', POINTS=128, HIDE_COORDINATES=.TRUE./

&DEVC XB=-0.020475,0.020475,0.0,0.0,0.155999,0.155999,
QUANTITY='W-VELOCITY', ID='Wmean30', POINTS=64, COORD_FACTOR=192.301 /
&DEVC XB=-0.020475,0.020475,0.0,0.0,0.155999,0.155999,
QUANTITY='W-VELOCITY', STATISTICS = 'RMS', ID='Wrms30', POINTS=64, HIDE_COORDINATES=.TRUE./
&DEVC XB=-0.020475,0.020475,0.0,0.0,0.155999,0.155999,
QUANTITY='CELL U', ID='Umean30', POINTS=64, HIDE_COORDINATES=.TRUE./
&DEVC XB=-0.020475,0.020475,0.0,0.0,0.155999,0.155999,
QUANTITY='CELL U', STATISTICS = 'RMS', ID='Urms30', POINTS=64, HIDE_COORDINATES=.TRUE./
&DEVC XB=-0.020475,0.020475,0.0,0.0,0.155999,0.155999,
QUANTITY='MASS FRACTION', SPEC_ID='PROPANE', ID='Fmean30', POINTS=64, HIDE_COORDINATES=.TRUE./
&DEVC XB=-0.020475,0.020475,0.0,0.0,0.155999,0.155999,
QUANTITY='MASS FRACTION', STATISTICS = 'RMS', SPEC_ID='PROPANE', ID='Frms30', POINTS=64, HIDE_COORDINATES=.TRUE./
&DEVC XB=-0.020475,0.020475,0.0,0.0,0.155999,0.155999,
QUANTITY='VISCOSITY', ID='VIS30', POINTS=64, HIDE_COORDINATES=.TRUE./
&DEVC XB=-0.020475,0.020475,0.0,0.0,0.155999,0.155999,
QUANTITY='SUBGRID KINETIC ENERGY', ID='KE30', POINTS=64, HIDE_COORDINATES=.TRUE./
&DEVC XB=-0.020475,0.020475,0.0,0.0,0.155999,0.155999,
QUANTITY='DENSITY', ID='RH030', POINTS=64, HIDE_COORDINATES=.TRUE./

&DEVC XB=0,0,0.0,0.0,0.0,0.1664,
QUANTITY='W-VELOCITY', ID='CL Wmean', COORD_FACTOR=192.301, POINTS=257/
&DEVC XB=0,0,0.0,0.0,0.0,0.1664,
QUANTITY='W-VELOCITY', ID='CL Wrms', STATISTICS = 'RMS', POINTS=257, HIDE_COORDINATES=.TRUE. /
&DEVC XB=0,0,0.0,0.0,0.0,0.1664,
QUANTITY='U-VELOCITY', ID='CL Umean', POINTS=257, HIDE_COORDINATES=.TRUE. /
&DEVC XB=0,0,0.0,0.0,0.0,0.1664,
QUANTITY='U-VELOCITY', ID='CL Urms', STATISTICS = 'RMS', POINTS=257, HIDE_COORDINATES=.TRUE. /
&DEVC XB=0,0,0.0,0.0,0.0,0.1664,
QUANTITY='MASS FRACTION', SPEC_ID='PROPANE', ID='CL Fmean', POINTS=257, HIDE_COORDINATES=.TRUE. /

```

```
&DEVC XB=0,0,0.0,0.0,0.0,0.1664,
QUANTITY='MASS FRACTION', SPEC_ID='PROPANE', STATISTICS = 'RMS', ID='CL Frms', POINTS=257, HIDE_COORDINATES=.TRUE. /
&DEVC XB=0,0,0.0,0.0,0.0,0.1664,
QUANTITY='SUBGRID KINETIC ENERGY', ID='CL KE', POINTS=257, HIDE_COORDINATES=.TRUE. /

&DEVC XB=-0.002438,0.002438,0,0,0.0000001,0.0000001,
QUANTITY='NORMAL VELOCITY', IOR=3, ID='Wmean BC', POINTS=32, COORD_FACTOR=192.301/
&DEVC XB=-0.002438,0.002438,0,0,0.0000001,0.0000001,
QUANTITY='DENSITY', ID='RHO BC', POINTS=32, HIDE_COORDINATES=.TRUE./
&DEVC XB=-0.002438,0.002438,0,0,0.0000001,0.0000001,
QUANTITY='MASS FRACTION', SPEC_ID='PROPANE', ID='MASS FRACTION BC', POINTS=32, HIDE_COORDINATES=.TRUE./

&TAIL/
```

Bibliography

- [1] G. Caird Ramsay. Fire safety engineering: Role in performance based codes. In *Proceedings of the Asia-Oceania Symposium of Fire Science and Technology (AOFST 3)*, pages 101–112. International Association for Fire Safety Science (IAFSS), 1988.
- [2] Nuclear Regulatory Commission. Voluntary fire protection requirements for light water reactors; adoption of nfpa 805 as a risk-informed, performance-based alternative. final rule. *Federal Register*, 69(175):33536, 2004.
- [3] United States Coast Guard. 2000 amendments to solas chapter ii-2. *Navigation and Vessel Inspection Circular (NVIC)*, 6, 2002.
- [4] United States Coast Guard. Outer continental shelf unites-fire and explosion analyses. notice of recommended interim voluntary guidelines. *Federal Register*, 78(175):55230, 2013.
- [5] Comparison of zone and cfd models. <http://www.enfp.umd.edu/research/fire-modeling/cfd>. Accessed March 25, 2015.
- [6] Philip J DiNenno. *SFPE handbook of fire protection engineering*. SFPE, 2008.
- [7] G. Forney K. McGrattan. *Fire Dynamics Simulator (Version 6), User's Guide*. National Institute of Standards and Technology, Gaithersburg, Maryland, July 2014. NIST Special Publication 1018.
- [8] G. Forney K. McGrattan. *Fire Dynamics Simulator (Version 6), Technical Guide*. National Institute of Standards and Technology, Gaithersburg, Maryland, July 2014. NIST Special Publication 1018.
- [9] Robert W Schefer. Data base for a turbulent, nonpremixed, nonreacting propane-jet flow. *Combustion Research Facility, Sandia National Laboratories, Livermore, CA. www.sandia.gov/TNF*, 1987.

- [10] FC Gouldin, RW Schefer, SC Johnson, and W Kollmann. Nonreacting turbulent mixing flows. *Progress in energy and combustion science*, 12(4):257–303, 1986.
- [11] T Djeridane, M Amielh, F Anselmet, and L Fulachier. Velocity turbulence properties in the near-field region of axisymmetric variable density jets. *Physics of Fluids (1994-present)*, 8(6):1614–1630, 1996.
- [12] A Gharbi, E Ruffin, F Anselmet, and R Schiestel. Numerical modelling of variable density turbulent jets. *International journal of heat and mass transfer*, 39(9):1865–1882, 1996.
- [13] Ching Jen Chen and Wolfgang Rodi. Vertical turbulent buoyant jets: a review of experimental data. *NASA STI/Recon Technical Report A*, 80:23073, 1980.
- [14] Ping Wang, Jochen Fröhlich, Vittorio Michelassi, and Wolfgang Rodi. Large-eddy simulation of variable-density turbulent axisymmetric jets. *International Journal of Heat and Fluid Flow*, 29(3):654–664, 2008.
- [15] EJ List. Turbulent jets and plumes. *Annual Review of Fluid Mechanics*, 14(1):189–212, 1982.
- [16] RW Dibble, V Hartmann, RW Schefer, and W Kollmann. Conditional sampling of velocity and scalars in turbulent flames using simultaneous ldv-raman scattering. *Experiments in Fluids*, 5(2):103–113, 1987.
- [17] Stephen B Pope. *Turbulent flows*. Cambridge university press, 2000.
- [18] Nicolas Jarrin, Sofiane Benhamadouche, Dominique Laurence, and Robert Prosser. A synthetic-eddy-method for generating inflow conditions for large-eddy simulations. *International Journal of Heat and Fluid Flow*, 27(4):585–593, 2006.
- [19] G. Forney K. McGrattan. *Fire Dynamics Simulator (Version 6), Validation Guide*. National Institute of Standards and Technology, Gaithersburg, Maryland, July 2014. NIST Special Publication 1018.
- [20] Stephen B Pope. Ten questions concerning the large-eddy simulation of turbulent flows. *New journal of Physics*, 6(1):35, 2004.